Calculation of the Electromagnetic Forces on the ASDEX Upgrade Vacuum Vessel on Disruption of the Plasma Current

H. Preis

IPP 1/229 January 1986

MAX-PLANCK-INSTITUT FÜR PLASMAPHYSIK

8046 GARCHING BEI MÜNCHEN

MAX-PLANCK-INSTITUT FÜR PLASMAPHYSIK

GARCHING BEI MÜNCHEN

Calculation of the Electromagnetic Forces on the ASDEX Upgrade Vacuum Vessel on Disruption of the Plasma Current

H. Preis

IPP 1/229 January 1986

Die nachstehende Arbeit wurde im Rahmen des Vertrages zwischen dem Max-Planck-Institut für Plasmaphysik und der Europäischen Atomgemeinschaft über die Zusammenarbeit auf dem Gebiete der Plasmaphysik durchgeführt.

Calculation of the Electromagnetic Forces on the ASDEX Upgrade Vacuum Vessel on Disruption of the Plasma Current

H. Preis

IPP 1/229

Abstract

This study investigates the magnetic field diffusion through the vacuum vessel of the ASDEX Upgrade tokamak that occurs on sudden disruption of the plasma current. Eddy currents are thereby produced in the vessel wall. Their time behaviour and distribution are determined. Furthermore, the vessel is permeated by various magnetic fields which, together with the eddy currents, exert magnetic forces in the vessel wall. These are also calculated. These numerical analyses are performed for two of the modes of operation envisaged for ASDEX Upgrade: the so-called limiter and single-null magnetic field configurations.

Contents

1. Introduction

As a tokamak is operated in pulsed mode, there are both steady-state and transient magnetic fields in it (see Fig. 1). These transient, i.e. time-varying, fields are produced during the excitation and de-excitation of the individual magnet systems and of the plasma. In addition, transient fields are caused by shifts in position of the ring-shaped plasma column or by unintentional fast disruption of the plasma current which can be triggered by instabilities in the plasma.

When time-varying magnetic fields permeate electrically conducting structures, they produce in accordance with the law of induction

$$\oint \vec{E} ds = -\frac{\partial \phi}{\partial t} \tag{1}$$

eddy currents, whose fields counteract the permeating field. Only after the eddy currents have decayed, the so-called diffusion process of the magnetic field comes to an end.

Here we investigate the magnetic field diffusion through the vacuum vessel of the ASDEX Upgrade tokamak [1] that occurs when there is a sudden disruption of the plasma current. In tokamaks this can cause the greatest rate of variation of a magnetic field, which according to eq. (1) produces maximum eddy current strengths. All other transient magnetic fields vary more slowly and are therefore not treated in this study. The eddy currents (EC) generated in the vessel walls during the diffusion process are analyzed in respect of their time behaviour and distribution. In conjunction with the static and dynamic magnetic fields these eddy currents exert magnetic forces

$$\vec{F} = \vec{G} \times \vec{B} \tag{2}$$

($\vec{G}$ eddy current density, $\vec{B}$ magnetic flux density) on the vessel which have a major influence on its design. It is therefore essential to determine the magnetic forces, their distribution and their time behaviour. This is done for the various modes of operation of ASDEX Upgrade which result from the use of different magnetic field configurations for plasma confinement, viz. the so-called limiter, and single-null configurations (L, SN) [1]. The choice of magnetic field configuration governs the shape of the plasma cross-section and the position of the plasma in the vacuum vessel. The L configuration is symmetric to the $z = 0$ plane, but not so the SN configuration. Accordingly, the plasma is positioned either symmetrically or asymmetrically to this plane. In SN operation the vessel is thus subjected to the most general load.

2. Calculation Method

Strict analysis of magnetic field diffusion calls for solution of the so-called diffusion equation

$$\Delta \vec{B} = \mu\kappa \frac{\partial \vec{B}}{\partial t} \tag{3}$$

($\vec{B}$ magnetic flux density, μ permeability, κ electrical conductivity). For diffusion processes in geometrically complicated apparatus, such as the vacuum vessel in the present case, solving this equation would be extremely complicated, even if the highly developed finite-element method were used [2]. This study therefore makes use of an approximation method, viz. the finite-element network (FEN) method, with which diffusion processes of magnetic fields can be calculated in good approximation [3].

The basic idea of the FEN is to subdivide the field permeated structure into finite elements which are then treated as branches of a passive RL network. All branches are inductively coupled with one another and with the external circuits which generate the diffusing field. In this investigation the external circuit is the plasma loop current. The eddy currents produced during the diffusion process can now be analyzed as transient branch currents of the network by the usual methods of network theory. The only limitation of the FEN is the requirement that $\vec{G} = \text{const}$ within a finite element. This requirement is satisfied in good approximation if the cross-sectional dimensions of the finite elements are chosen smaller than the penetration depth $\delta = (\mu\kappa\omega)^{-1/2}$. The FEN is the basis of the FEDIFF code, with which diffusion processes can be calculated in four basic steps:

1. Subdivision of the structure into finite elements and calculation of their inductances and ohmic resistances. Development of the passive RL network.
2. Calculation of the mutual inductances between the branches of the RL network and the external field-generating circuits.
3. Solution of the differential equation of the network and calculation of the time evolution and distribution of the eddy currents.
4. Calculation of the magnetic field of the eddy currents.

On the basis of the above-described analysis it is possible in a further step to determine the magnetic forces

$$\vec{F} = \vec{G} \times \vec{B} = GB \sin(\sphericalangle \vec{G}, \vec{B}) = \begin{vmatrix} \vec{e}_x & \vec{e}_y & \vec{e}_z \\ G_x & G_y & G_z \\ B_x & B_y & B_z \end{vmatrix} \tag{4}$$

which act on the field-permeated structure during the diffusion process. In eq. (4), $\vec{G}$ is the vector of the eddy current density and $\vec{B}$ the vector of the magnetic flux density, which in the case of a tokamak is composed of the flux densities of the toroidal field (TF), the equilibrium field (EF) and the eddy current field (ECF) itself. To produce the field configurations under consideration, the following current strengths are required in the individual magnet systems (Fig. 1):

a. Limiter Configuration

Plasma current(No. 12)	$I_p = 2\,\mathrm{MA}$,
Equilibrium coils (No. 2–7):	$I_2 = I_3 = 2\,\mathrm{MA}$,
	$I_4 = I_5 = -0.24\,\mathrm{MA}$,
	$I_6 = I_7 = -1.3\,\mathrm{MA}$,
Toroidal field coils (No. 10):	$I_{10} = 1.675\,\mathrm{MA}$,
in each of the 16 coils.	

b. Single-null configuration

Plasma current (No. 12):	$I_p = 1.6\,\mathrm{MA}$,
Equilibrium field coils (No. 2–7):	$I_2 = 1.36\,\mathrm{MA}$,
	$I_3 = 4.0\,\mathrm{MA}$,
	$I_4 = -0.5\,\mathrm{MA}$,
	$I_5 = 1.73\,\mathrm{MA}$,
	$I_6 = -0.72\,\mathrm{MA}$,
	$I_7 = -0.56\,\mathrm{MA}$,
Toroidal field coils (No. 10):	$I_{10} = 1.392\,\mathrm{MA}$,
in each of the 16 coils.	

The numerical values given are current strengths which have to flow through the entire winding cross-section of the particular coil concerned.

These magnetic fields and the magnetic forces acting in the vessel wall are calculated with the HEDO 2 code [4], which was coupled with the FEDIFF code for this purpose.

2.1 Modelling of the Vacuum Vessel

The vessel, made of non-magnetizable, austenitic steel AISI 304 LN, is in the form of a torus and is symmetric with respect to its equatorial plane. It is composed of 8 equal octants each with two equal segments which are bolted together by means of flange connections (Fig. 2). The shells located between the flanges have surfaces with simple curvature, i.e. they form in the toroidal direction a closed polygon whose corners are located in the symmetry planes of the TF coils (Fig. 3). Furthermore, the 16 segments of the vessel have the cross-sectional dimensions shown in section AB of Fig. 3. The individual octants are welded together (octant connection), but the flange connections between the two segments of an octant are designed to provide electrical insulation (Fig. 4). This prevents the ring-shaped vacuum vessel from acting as a short circuit winding of the OH transformer (Fig. 1). Owing to the insulation material it is not readily possible to make these bolted connections UHV-tight (UHV = ultra high vacuum, $p \lesssim 10^{-7}$ mb). They are therefore covered with high-resistance bellows welded in between the segments (Fig. 4). When dimensioning the bellows it must be ensured that the ohmic resistance of the vessel in the toroidal direction is high enough to guarantee ignition of the plasma by the OH transformer.

The development of a calculation model matching the FEN made use of the symmetries of the vessel, ignoring the vessel ports. Accordingly, the investigation can be conducted on one segment, as the smallest symmetric part of the vessel. A segment is composed of the shell part, the flange and the adjoining bellows (Fig. 5). These components of different shape and wall thickness are treated in the computation model as one segment subdivided into three regions of equal wall thickness. In the computation model different shapes and wall thicknesses of the original components are taken into account by means of the specific resistance. That is, the toroidal and poloidal directions of the three segment regions are each assigned a different specific resistance. The latter is fixed for each of the three segment regions of the model, so that the ohmic resistances of the original and of the model are equal (Table I).

The segment considered, consisting of the regions of bellows, flange and shell, now has to be represented as an electrical network in accordance with the FEN. For this purpose the vessel wall is subdivided into finite elements of finite thickness, each element corresponding to a network branch [3]. The elements aligned in the toroidal and poloidal directions are referred to as u- and v-plates, respectively. Elements aligned normal to the surface are ignored since the vessel wall can be regarded as thin. It is assumed that per vessel segment there are 9 u-plates in the toroidal direction and 28 in the poloidal direction, i.e. a total of $9 \times 28 = 252$, which thus fixes the number of v-plates at

Item	Original	Model
a) Bellows		
Stretched length	0.2448m	0.010m
Wall thickness	0.0009m	0.015m
Circumference length in ϑ-direction	6.76m	
Specific resistivity:		
in φ-direction	$0.73 \cdot 10^{-6} \Omega\,\mathrm{m}$	$0.298 \cdot 10^{-3} \Omega\,\mathrm{m}$
in ϑ-direction	$0.73 \cdot 10^{-6} \Omega\,\mathrm{m}$	$0.5 \cdot 10^{-6} \Omega\,\mathrm{m}$
b) Flange		
Wall thickness	0.05m	0.015m
Specific resistivity	$0.73 \cdot 10^{-6} \Omega\,\mathrm{m}$	$0.219 \cdot 10^{-6} \Omega\,\mathrm{m}$

Table 1: Conversion of original sizes into model sizes

$10 \times 28 = 280$. Of the nine u-plates in a row one is assigned to the bellows region, three to the flange region, and five to the shell region of the segment. All of the plates together thus form a two-dimensional electrical network with 532 branches and 253 meshes (see Fig. 6). The following symmetries [3] have to be considered when modelling the network:

- The meridional separating planes of symmetry between the segments are so-called e-mirrors, i.e. the eddy current lines are perpendicular to these planes.
- The equatorial plane of the torus is a so-called s-mirror (the eddy current lines are tangential to this plane) if the field of the plasma current is symmetric to this plane. If this condition is satisfied, the eddy current analysis can be restricted to the top half of the segment. The network required for this purpose then consists of 256 branches with 118 meshes.

Although the eddy current analysis can be restricted to one segment of the torus in view of the given symmetry, the interaction prevailing between the segments still has to be taken into account. In the FEN this interaction is formally expressed by the mutual inductances, which have to be calculated between the circuits of all segments of the vessel.

2.2 Simulation of the Diffusing Magnetic Field

The magnetic field of the plasma current as the exciting field of the RL network developed in Sec. 2.1, has to be simulated. The current flowing in the ring-shaped plasma column is approximated by a line current, which can be thought of as running along the center of the plasma and which is magnetically coupled with the RL network via the mutual inductances. In this approximation the influence of the elongated plasma cross-section on the eddy current distribution is not taken into account. However, test calculations, in which the distributed plasma current was reproduced by a number of line currents, have shown that no essentially different current distributions occur on the vessel. Depending on the mode of operation of ASDEX Upgrade, i.e. limiter or single-null configuration, the center of the plasma is located either in the $z = 0$ plane or it is displaced by $z_s = 0.15\,\mathrm{m}$ from it (see Fig. 8). For the two modes of operation stated, the sudden breakdown of the plasma current which typically occurs as a result of plasma disruption is investigated. For this purpose it is assumed that on disruption the plasma current goes linearly to 0 in accordance with

$$\dot{i}_p = \begin{cases} I_{po} - (I_{po}/t_d) \cdot t & \text{for } 0 \le t \le t_d \\ 0 & \text{for } t > t_d \end{cases} \tag{5}$$

where $I_{po} = 2\,\mathrm{MA}$, $t_d = 5\,\mathrm{ms}$ for the limiter configuration and $I_{po} = 1.6\,\mathrm{MA}$, $t_d = 4\,\mathrm{ms}$ for the single-null configuration. These numerical values are based on experimental results.

In addition, the disruption of the plasma current is analyzed for the case where the plasma is in the vertically displaced position $z_s = 0.3\,\mathrm{m}$. In this position the separatrix is just touching the vessel wall. Such shift is conceivable if the plasma position control were to fail. For the current disruption it is assumed that it conforms to that of the single-null configuration.

3. Results

First a few basic aspects of the diffusion process considered here are treated in order to make the results more readily understood. During magnetic field diffusion eddy currents are generated in the vessel wall whose amplitude depends on the rate of change $\frac{d\phi}{dt}$ of the diffusing field and whose decay time is governed by the vessel time constant. That is, the diffusion process does not take place in an infinitely short time but terminates only when the eddy currents have decayed. A major influence is exerted on the diffusion process by the high-resistance bellows of the vessel. In a toroidal vessel of uniform

structure the eddy currents flow exclusively in the toroidal direction, this being in the direction of the plasma current if the latter is subject to negative change. The current lines are thus concentric circles about the axis of symmetry of the torus. If the vessel has meridional insulating gaps, it is no longer possible for the eddy currents to close upon themselves as toroidal loop currents. This results in so-called saddle currents, which form closed current lines both in the top and bottom halves of torus segments defined by insulating gaps (Fig. 3). The dividing lines between the current eddies of the top and bottom segment halves are then only located in the equatorial plane $z = 0$, if the diffusing field is symmetric to the latter. In the ASDEX Upgrade vacuum vessel, high-resistance bellows are used as connecting elements between the individual vessel octants instead of insulating connections. As a consequence, the eddy currents within each octant now consist of two components, the toroidal loop currents and the saddle currents. Through the bellows, on the other hand, it is just the toroidal loop currents that flow, the amplitude of these being essentially governed by the ohmic resistance of the bellows.

3.1. Time Behaviour and Distribution of the Eddy Currents

Figure 7 shows the time behaviour of the eddy currents i_t and i_s on disruption of the plasma current in accordance with eq. (5) for the limiter configuration. On the basis of eq. (5), the eddy currents show analogous time behaviour for the single-null and the displaced single-null configuration. The notation is as follows:

i_t the sum of all toroidal loop currents which can be summed in a vertical section through a bellows connection along the poloidal vessel circumference. For reasons of symmetry there exists in this sectional plane only currents which flow in the toroidal direction.

i_s the sum of all saddle currents which flow in the top and bottom vessel halves within an octant. The sum can be formed along section AB of Fig. 10.

The time constants characteristic of the vessel

$$\tau_t = 7\,\text{ms}$$

$$\tau_s = 10\,\text{ms}$$

can be read directly from the curves shown in Fig. 7.

The eddy current distribution, which on disruption of the plasma current in the single-null mode assumes the most general form, is shown in Fig. 9. Unlike in the limiter configuration, the diffusing field in this case is no longer symmetric to the $z = 0$ plane.

Accordingly, the eddy current distribution, which is represented in Fig. 9 on the developed surface of a vessel octant, no longer has top-bottom symmetry either. The developed surface is actually wedge-shaped, but it is given here in distorted representation as a rectangle for the sake of clarity. The angle φ runs in the direction of the toroidal circumference, and the arc length s_ϑ in the direction of the poloidal circumference. The arc length s_ϑ increases in the clockwise direction, starting at the point on the vessel octant furthest from the torus axis. The bellows connections are located in the planes $\varphi_n = n \cdot \pi/4$ for $n = 0.1, ...7$, which at the same time are so-called e-mirrors.

The eddy current distribution which is represented in Fig. 9 at the time of maximum current intensity ($t = 4\,\mathrm{ms}$), shows that:

- the current intensity in vessel regions near the plasma is larger than that further away,
- the current distribution on the top octant half does not correspond to that of the bottom half,
- the eddy currents in the symmetry planes $\varphi_n = n \cdot \pi/8$, n=0.1,2...15 just have components in the φ direction.

Figure 10 shows the distribution of the saddle currents i_s in the same region. This is obtained when the toroidal loop currents i_t are subtracted from the currents in the distribution shown in Fig. 9. The eddy currents produced, which close upon themselves within a vessel octant, are clearly evident.

3.2. Magnetic Forces

In this section the magnetic forces on the vacuum vessel calculated according to eq. (4) are evaluated. To discuss their time behaviour first of all, it is again pointed out that the magnetic flux density in eq. (4) consists of three components:

$$\vec{B} = \vec{B}_{TF} + \vec{B}_{EF} + \vec{B}_{ECF}. \tag{6}$$

The first two sum terms, the dominant ones, denote the steady-state flux densities of the TF and the EF, respectively. In contrast, the flux density $\vec{B}_{ECF}$ of the ECF varies in proportion to the eddy current density $\vec{G}$, so that the partial forces $\vec{F}_{TF}$ and $\vec{F}_{EF}$ emanating from the TF and EF, respectively, vary in proportion to $\vec{G}$, and the partial forces $\vec{F}_{ECF}$ as its square. The vessel is thus subjected to the magnetic forces of a dynamic load. They attain their maximum values at the time of maximum current

density. In further investigations the maximum forces are regarded. For this purpose the local coordinate system ϑ, φ, n given in Fig. 8 is used. The distribution of the total magnetic forces exerted

$$\vec{F} = \vec{F}_{TF} + \vec{F}_{EF} + \vec{F}_{ECF} = \vec{e}_{\varphi} F_{\varphi} + \vec{e}_{\vartheta} F_{\vartheta} + \vec{e}_{n} F_{n} \tag{7}$$

is the same in each vessel octant since the magnetic fields and the eddy current distribution of the three configurations considered here are cyclically symmetric with the period $\pi/4$ about the z-axis. That is, two adjacent octants are symmetrically loaded with respect to the planes of symmetry $\varphi = \varphi_n$. This does not apply, however, to the two octant segments of symmetric structure, which, in the limiter case, with respect to the plane of symmetry $\varphi = \varphi_n$, are symmetrically loaded by the partial forces $\vec{F}_{EF}$ and $\vec{F}_{ECF}$, and antisymmetrically by the partial forces $\vec{F}_{TF}$

In both the SN and displaced SN configurations the plasma position and hence the eddy current distribution as well are not symmetric to the $z = 0$ plane. The forces acting on the top half of the vessel are no longer equal to those acting on the bottom half. There are resulting forces $\vec{F}_{\varphi}$ and $\vec{F}_{z}$ exerted on the vessel in the toroidal and vertical directions, respectively. These are forces to which the supports react. The force $\vec{F}_{\varphi}$ generates a torque M_z which causes the toroidal vessel to rotate abbout the z-axis. In numerical terms, the supports react as follows:

SN configuration	$\vec{F}_z = 5045\,\mathrm{N}$,	$\vec{M}_z = 7191\,\mathrm{Nm}$ per octant
displaced SN configuration	$\vec{F}_z = 35063\,\mathrm{N}$,	$\vec{M}_z = 14433\,\mathrm{Nm}$ per octant

Due to the symmetric position of the plasma in the L-case, no resulting forces occur.

3.2.1 Limiter Configuration

In this mode the magnetic fields and the eddy current distribution are symmetric not only to the planes $\varphi = \varphi_n$ but also to the horizontal plane z=0. This results in a segment being loaded symmetrically; likewise with respect to z=0, by the partical forces $\vec{F}_{EF}$ and $\vec{F}_{ECF}$ and antisymmetrically by the partial forces $\vec{F}_{TF}$.

The normal component F_n is taken as an example first to show how the load of a segment is composed of symmetrically and antisymmetrically acting forces in relation to the symmetry planes $z = 0$. The symmetric components $\vec{F}_{EF}$ and$\vec{F}_{ECF}$ are produced by the interaction of the eddy currents with the EF and the ECF (see Fig. 11a+b), while

the antisymmetric component $\vec{F}_{TF}$ is produced by the interaction of eddy currents and TF (see Fig. 11c). The distribution of the total force represented in Fig. 11d then results from all of these components superposed. It does not have top-bottom symmetry because it contains both symmetric and antisymmetric components. The force distribution in the adjacent segment is diametrically opposite to the foregoing one with respect to the $z = 0$-plane. The normal line forces along the poloidal vessel circumference that are shown in Fig. 11a–d are obtained from those of a segment when these are summed each time at the position of the marked vector along a toroidally running line. The distributions of the poloidally and toroidally directed line forces F_ϑ and F_φ are obtained in a similar way. They are plotted in Figs. 12 and 13 versus the developed poloidal circumference of the vessel. In addition, the total force per unit area is represented as a contour line plot on the developed surface of a segment. As contour lines cannot give any information on the direction of the force but merely fix locations of equal magnitude, these plots have to be given for each component of the force (see Figs. 14–16).

3.2.2 Single-null Configuration

In this configuration neither the external magnetic field nor the eddy current distribution is symmetric to the $z = 0$ plane. It thus follows that the force distributions of two adjacent segments are no longer diametrically opposite to one another with respect to the $z = 0$-plane, as in the limiter case. This is evident in both Fig. 17 and Figs. 18–23, in which the force distributions of segments 1 and 16 of an octant are represented as in Sec. 3.2.1. On the other hand, the cyclic symmetry about the z axis of field and currents is preserved, so that all octants are subjected to one and the same load.

Comparison of Figs. 11 and 17 shows that the amplitudes of the forces in the single-null configuration are smaller than those in the limiter configuration. This can be attributed to the smaller flux densities of the TF in single-null operation. Furthermore, the distribution functions to be compared show slight displacements of the zero passages relative to one another, this being due to the change in plasma position.

3.2.3 Displaced Single-null Configuration

As mentioned in Sec. 2.2, in this disturbed case the plasma center is located at the largest conceivable distance $z_s = 0.3\,\mathrm{m}$ from the symmetry plane $z = 0$. If the plasma current is disrupted in this position, the magnetic field diffusing through the vessel wall attains the largest possible asymmetry with respect to the plane $z = 0$. It is therefore of interest to determine the distribution of the magnetic forces. This is done in Figs. 24–29

in the form of representation already used and described above. The calculations do not take into account the diffusion processes occurring during the motion of the plasma into this asymmetric position. These would produce eddy currents which flow in the direction opposite to those in the case of current disruption. As a result, the amplitudes of the total current and hence those of the forces as well decrease.

4. Conclusions

The calculations described here did not take into account the vessel ports and the so-called passive stabilizing conductors (see Fig. 1). The results presented are, of course, subject to errors owing to these omissions. Taking into account the stabilizing conductors and the vessel ports – particularly those of the present size – the distribution of the vessel currents will locally be influenced, which could lead to locally higher magnetic forces. To make the results more reliable in this respect, it would be necessary to make diffusion calculations that do not neglect these aspects. This is possible in principle, but not without elaborating the FEDIFF code. Ultimately, it will prove correct to await the results of mechanical strength calculations before deciding whether detailed diffusion calculations are necessary.

As the three examples calculated show, the vessel in the limiter case is subjected to the largest electromagnetic load. These results are therefore used as input data for the mechanical strength calculation.

Acknowledgement

The author wishes to thank Shü-chuan Cha for programming an evaluation routine for graphically representing the force distribution calculated with FEDIFF and HEDO 2.

References

[1] ASDEX Upgrade Design Team and Tokamak Theory Group. *ASDEX Upgrade, Definition of a Tokamak Experiment with Reactor-Compatible Poloidal Divertor*. IPP Report 1/197, Max-Planck-Institut für Plasmaphysik, Garching (March 1982).

[2] U. Jeske. *Dreidimensionale Wirbelstromberechnung mit Hilfe der Galerkin-Methode der Finiten Elemente*. KFK Report 03.03.01p 03D, Kernforschungszentrum Karlsruhe (Sept. 1987).

[3] H. Preis. *Die Finite-Element-Netzwerksmethode für dreidimensionale Wirbelstromberechnungen in Experimenten zur kontrollierten Kernfusion*. Archiv für Elektrotechnik 65 (1982) 233-239.

[4] P. Martin, H. Preis. *Programmbeschreibung und Benutzeranleitung zum Magnetfeld-Computerprogramm HEDO 2*. IPP Report III/34, Max-Planck-Institut für Plasmaphysik, Garching (April 1977).

Figure Captions

Fig. 1. Vertical half cross-section of the coil system of the ASDEX Upgrade tokamak. 1 OH coils, 2–7 equilibrium field coils, 8 control coils, 9 passive stabilizing conductors, 10 TF coil, 11 vacuum vessel, 12 plasma.

Fig. 2. Partial view of the toroidal ASDEX Upgrade vacuum vessel.

Fig. 3. Partial cross-section through the equatorial plane of the vacuum vessel. 1 bellows connection, 2 octant connection, i_s current lines of the saddle currents.

Fig. 4. Cross-section of the vessel wall at the insulating flange. 1 vessel wall, 2 electrical insulation, 3 bellows, 4 thermal insulation.

Fig. 5. Cross-section of the wall of a vessel segment. a actual cross-section; b cross-section of the calculation model. 1 shell, 2 flange, 3 bellows, 4 octant connection, 5 bellows connection.

Fig. 6. Partial network for eddy current calculations. u, v branches aligned in the φ and ϑ directions, K nodes, m mesh, i_p plasma current, ϕ_{pm} magnetic flux of i_p which penetrates the m-th mesh.

Fig. 7. Time behaviour of the eddy currents in the limiter configuration. i_t sum current in the toroidal direction, i_s saddle current.

Fig. 8. Plasma and vessel cross-sections with global x, y z and local ϑ, φ, n coordinates.

Fig. 9. Distribution of the eddy currents on the developed surface of a vessel octant at the time t=5ms (single-null configuration). s_ϑ arc length in ϑ direction.

Fig. 10. Distribution of the saddle currents on the developed surface of a vessel octant at time t=5ms (single-null configuration). s_ϑ arc length in ϑ direction.

Fig. 11. Distribution of the normal force F_n on segment 1 (L configuration). Interaction of the EC with the: a EF, b ECF, c TF, d EF + ECF + TF.

Fig. 12. Distribution of the poloidally directed total force F_ϑ on segment 1 (L configuration).

Fig. 13. Distribution of the toroidally directed total force F_φ on segment 1 (L configuration).

Fig. 14. Contour lines of the total force F_ϑ (L configuration): a on the top half of segment 1, b on the bottom half of segment 1.

Fig. 15. Contour lines of the total force F_φ (L configuration): a on the top half of segment 1, b on the bottom half of segment 1.

Fig. 16. Contour lines of the total normal force F_n (L configuration): a on the top half of segment 1, b on the bottom half of segment 1.

Fig. 17. Distribution of the total normal force F_n (SN configuration): a on segment 1, b on segment 16.

Fig. 18. Contour lines of the total force F_ϑ (SN configuration): a on the top half of segment 1, b on the top half of segment 16.

Fig. 19. Contour lines of the total force F_ϑ (SN configuration): a on the bottom half of segment 1, b on the bottom half of segment 16.

Fig. 20. Contour lines of the total force F_φ (SN configuration): a on the top half of segment 1, b on the top half of segment 16.

Fig. 21. Contour lines of the total force F_φ (SN configuration): a on the bottom half of segment 1, b on the bottom half of segment 16.

Fig. 22. Contour lines of the total normal force F_n (SN configuration): a on the top half of segment 1, b on the top half of segment 16.

Fig. 23. Contour lines of the total normal force F_n (SN configuration): a on the bottom half of segment 1, b on the bottom half of segment 16.

Fig. 24. Contour lines of the total force F_ϑ (displaced SN configuration): a on the top half of segment 1, b on the top half of segment 16.

Fig. 25. Contour lines of the total force F_ϑ (displaced SN configuration): a on the bottom half of segment 1, b on the bottom half of segment 16.

Fig. 26. Contour lines of the total force F_φ (displaced SN configuration): a on the top half of segment 1, b on the top half of segment 16.

Fig. 27. Contour lines of the total force F_φ (displaced SN configuration): a on the bottom half of segment 1, b on the bottom half of segment 16.

Fig. 28. Contour lines of the total normal force F_n (displaced SN configuration): a on the top half of segment 1, b on the top half of segment 16.

Fig. 29. Contour lines of the total normal force F_n (displaced SN configuration): a on the bottom half of segment 1, b on the bottom half of segment 16.

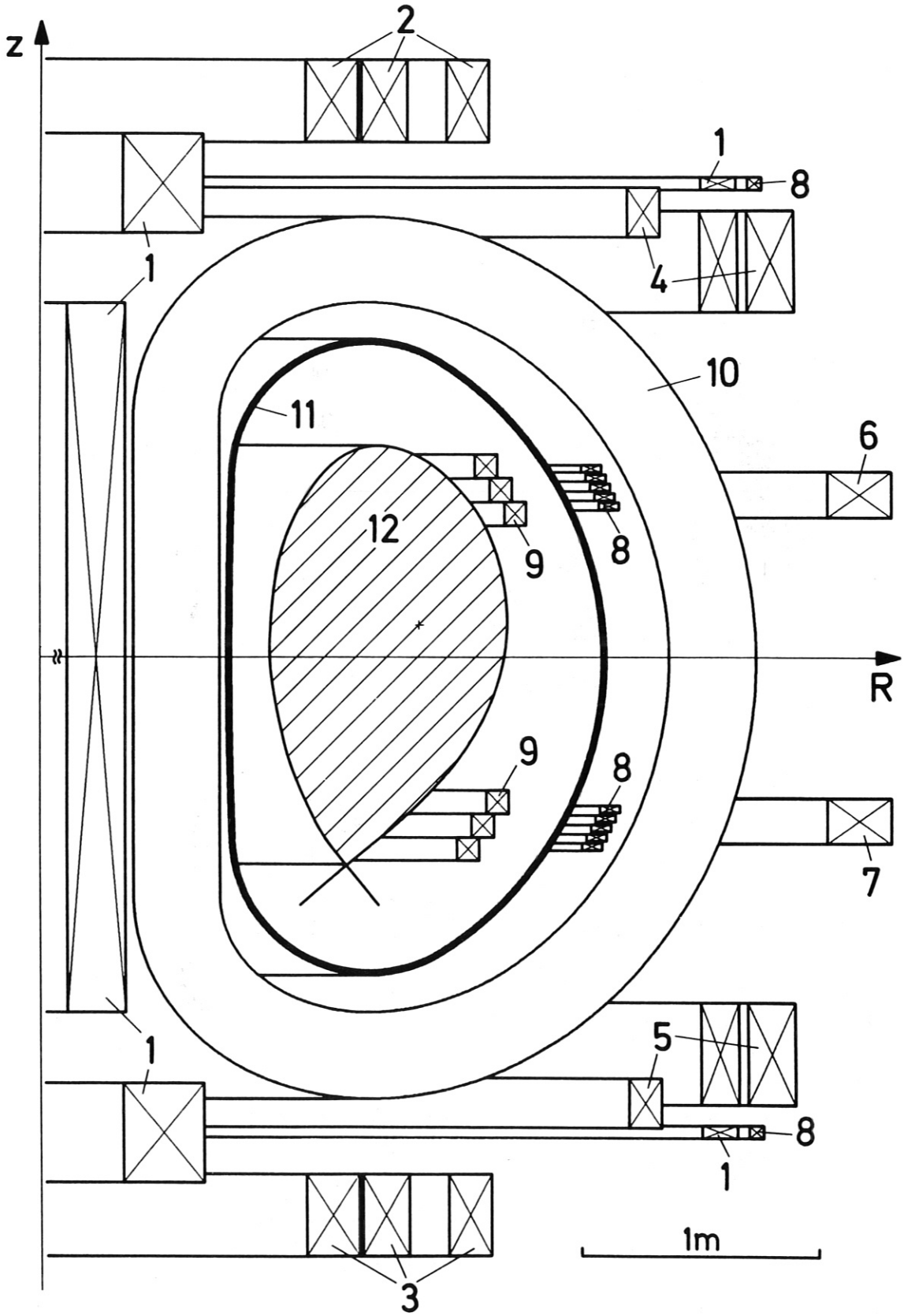

Fig. 1. Vertical half cross-section of the coil system of the ASDEX Upgrade tokamak. 1 OH coils, 2–7 equilibrium field coils, 8 control coils, 9 passive stabilizing conductors, 10 TF coil, 11 vacuum vessel, 12 plasma.

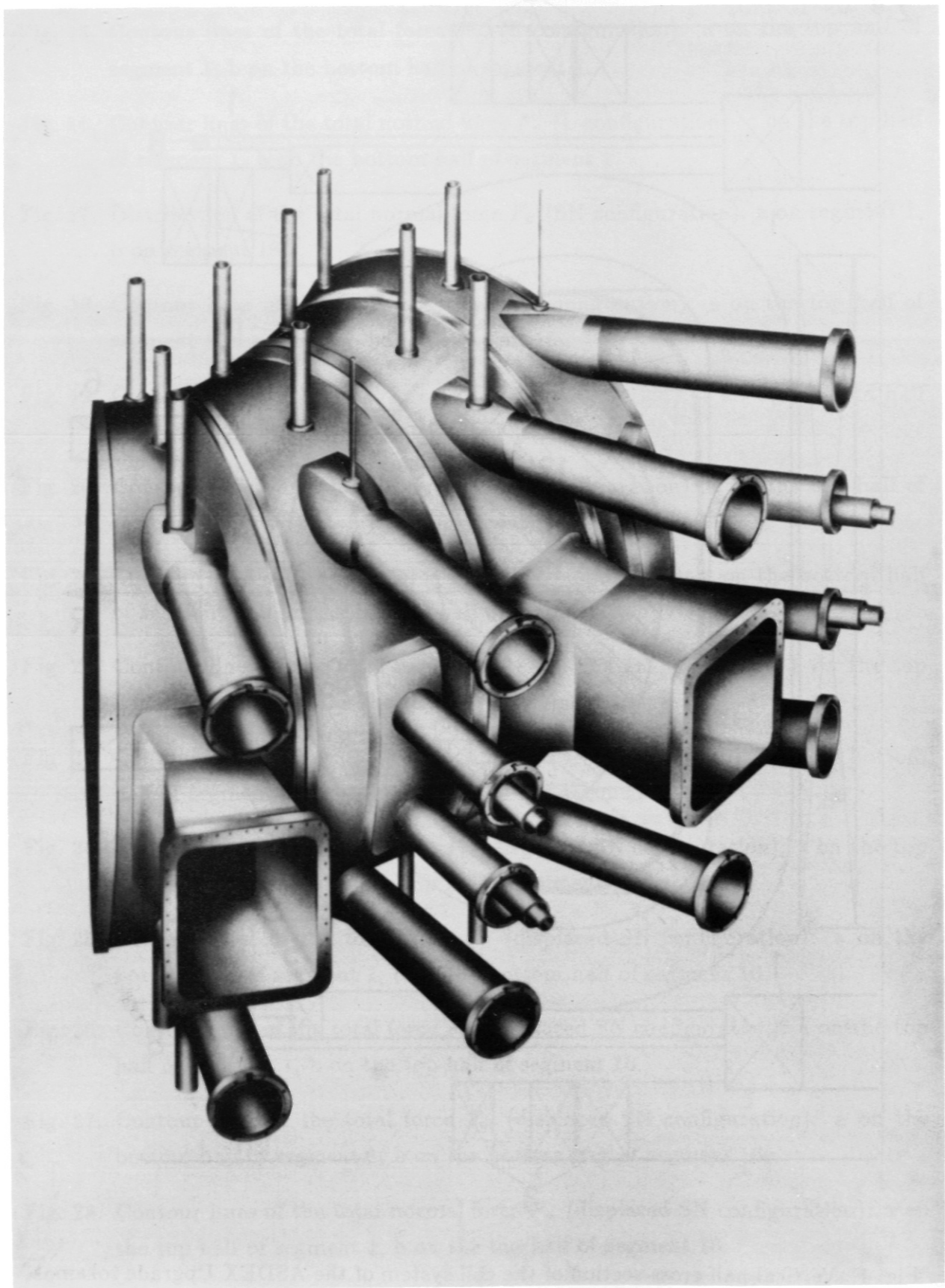

Fig. 2. Partial view of the toroidal ASDEX Upgrade vacuum vessel.

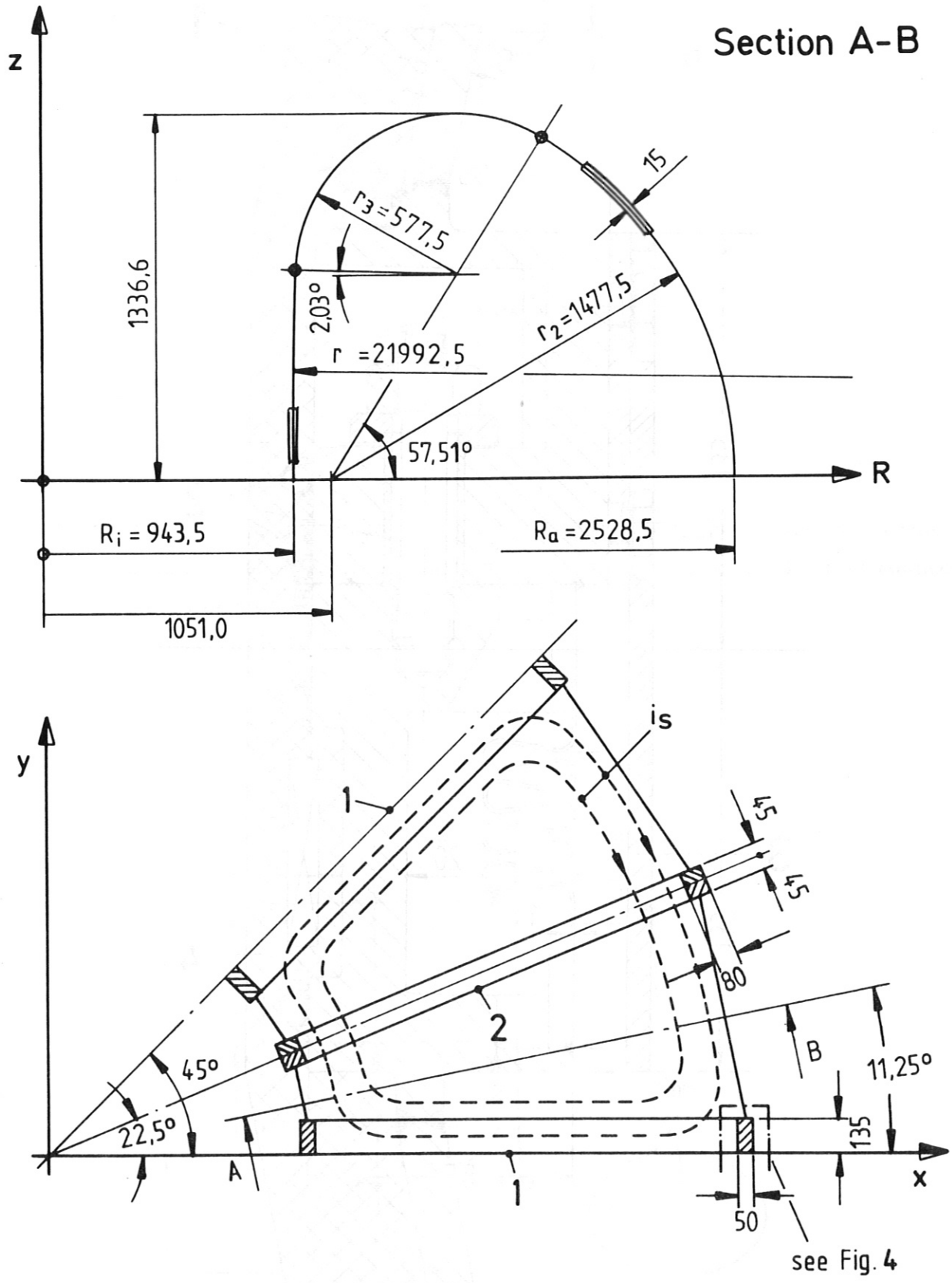

Fig. 3. Partial cross-section through the equatorial plane of the vacuum vessel. 1 bellows connection, 2 octant connection, i_s current lines of the saddle currents.

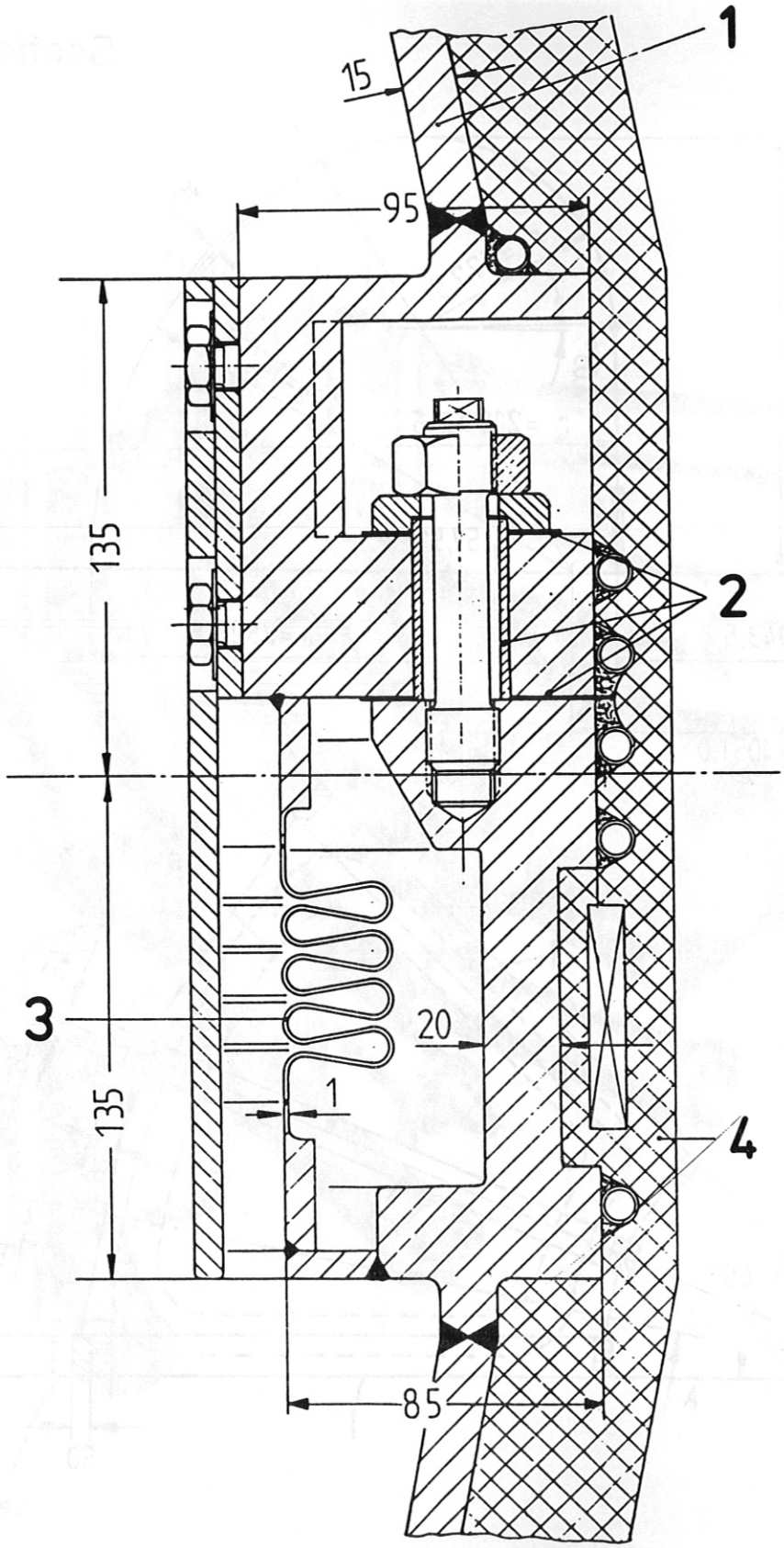

Fig. 4. Cross-section of the vessel wall at the insulating flange. 1 vessel wall, 2 electrical insulation, 3 bellows, 4 thermal insulation.

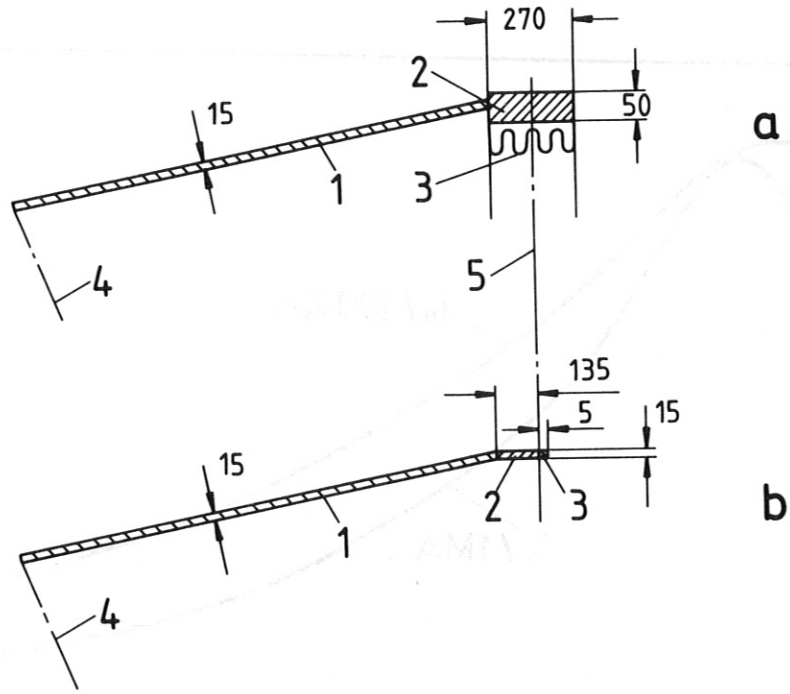

Fig. 5. Cross-section of the wall of a vessel segment. a actual cross-section; b cross-section of the calculation model. 1 shell, 2 flange, 3 bellows, 4 octant connection, 5 bellows connection.

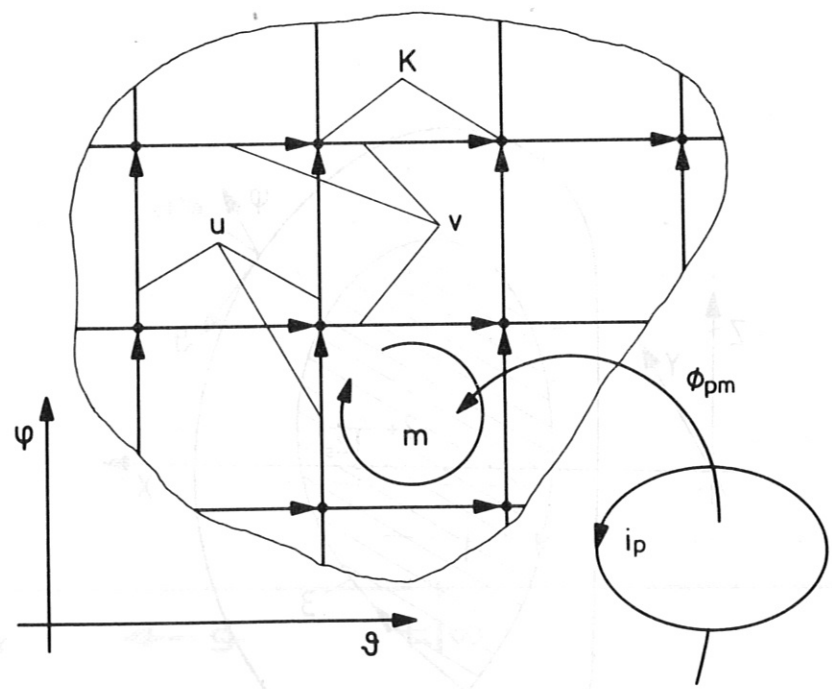

Fig. 6. Partial network for eddy current calculations. u, v branches aligned in the φ and ϑ directions, K nodes, m mesh, i_p plasma current, ϕ_{pm} magnetic flux of i_p which penetrates the m-th mesh.

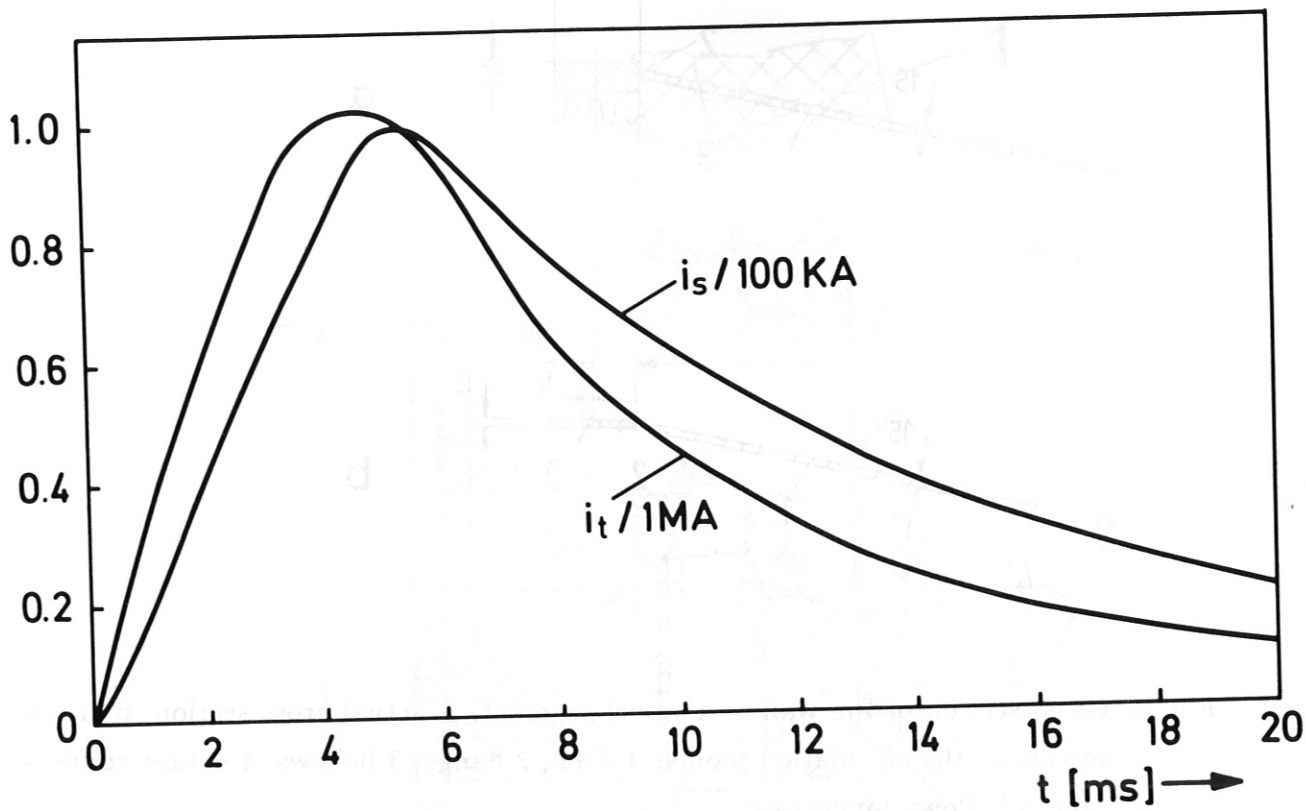

Fig. 7. Time behaviour of the eddy currents in the limiter configuration. i_t sum current in the toroidal direction, i_s saddle current.

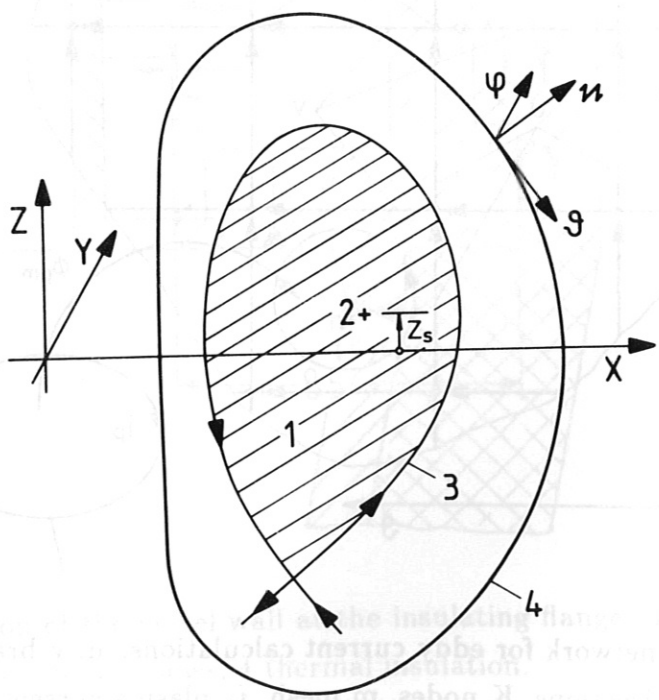

Fig. 8. Plasma and vessel cross-sections with global x, y z and local ϑ, φ, n coordinates.

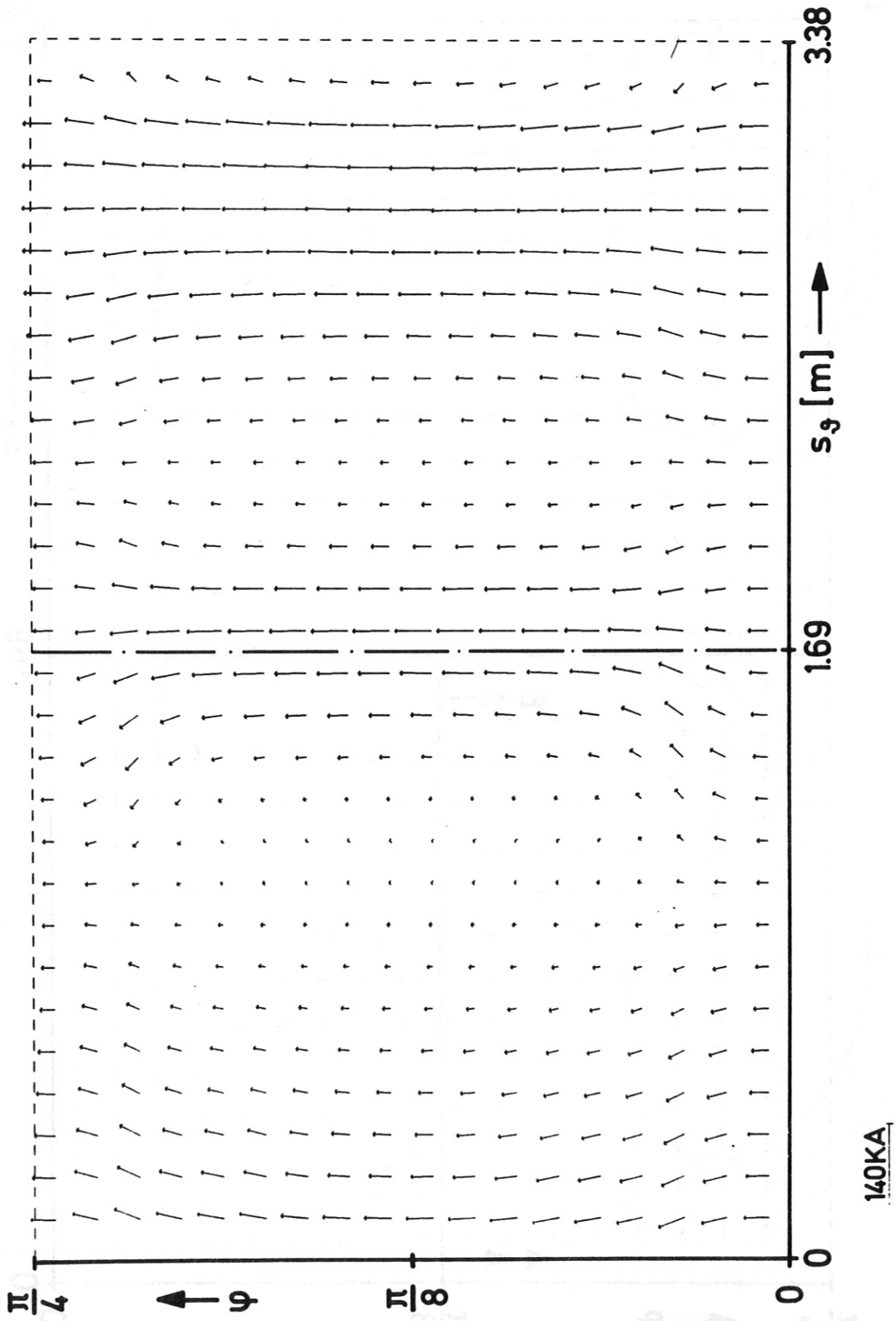

Fig. 9. Distribution of the eddy currents on the developed surface of a vessel octant at the time t=5ms (single-null configuration). s_ϑ arc length in ϑ direction.

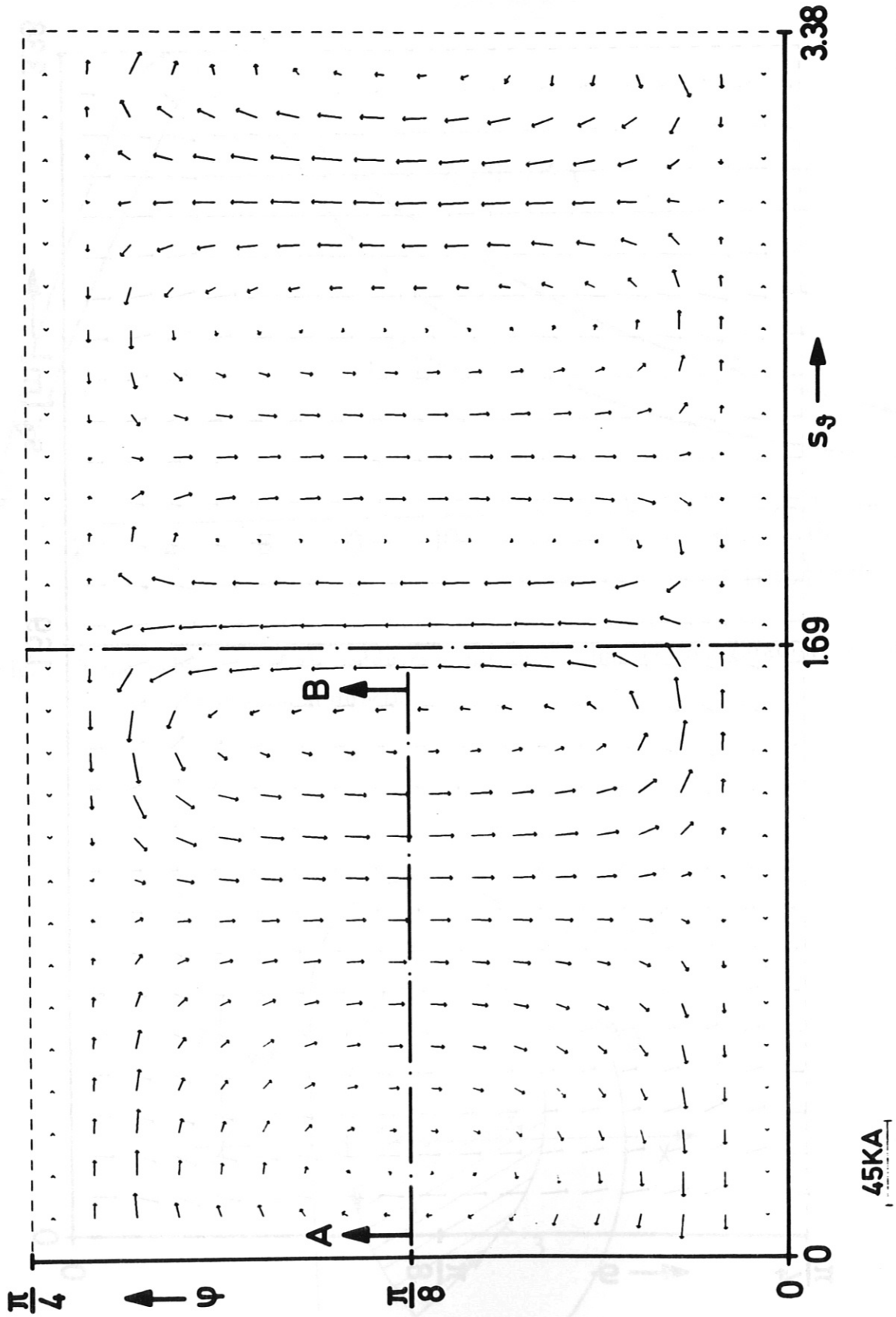

Fig. 10. Distribution of the saddle currents on the developed surface of a vessel octant at time t=5ms (single-null configuration). s_ϑ arc length in ϑ direction.

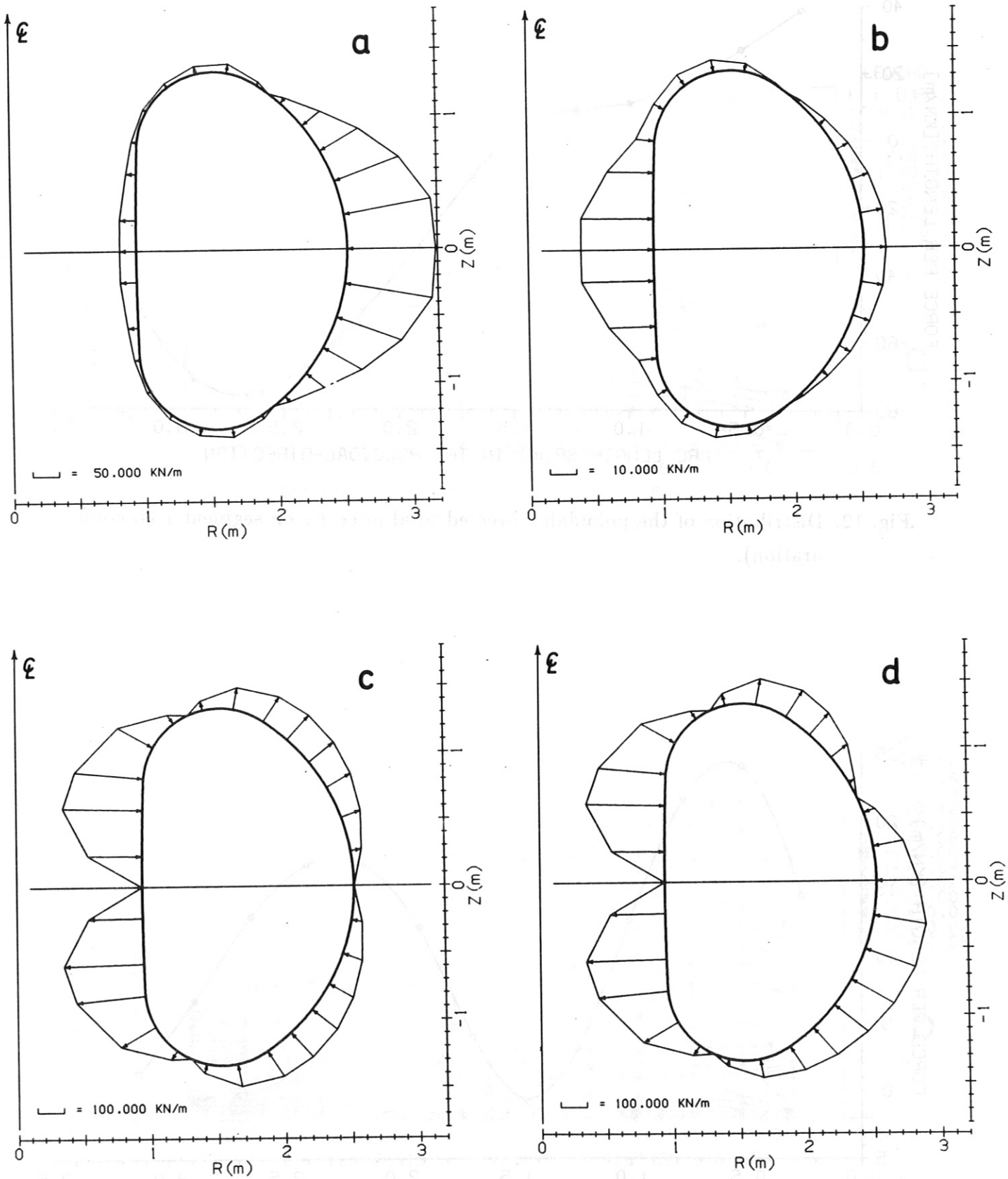

Fig. 11. Distribution of the normal force F_n on segment 1 (L configuration). Interaction of the EC with the: a EF, b ECF, c TF, d EF + ECF + TF.

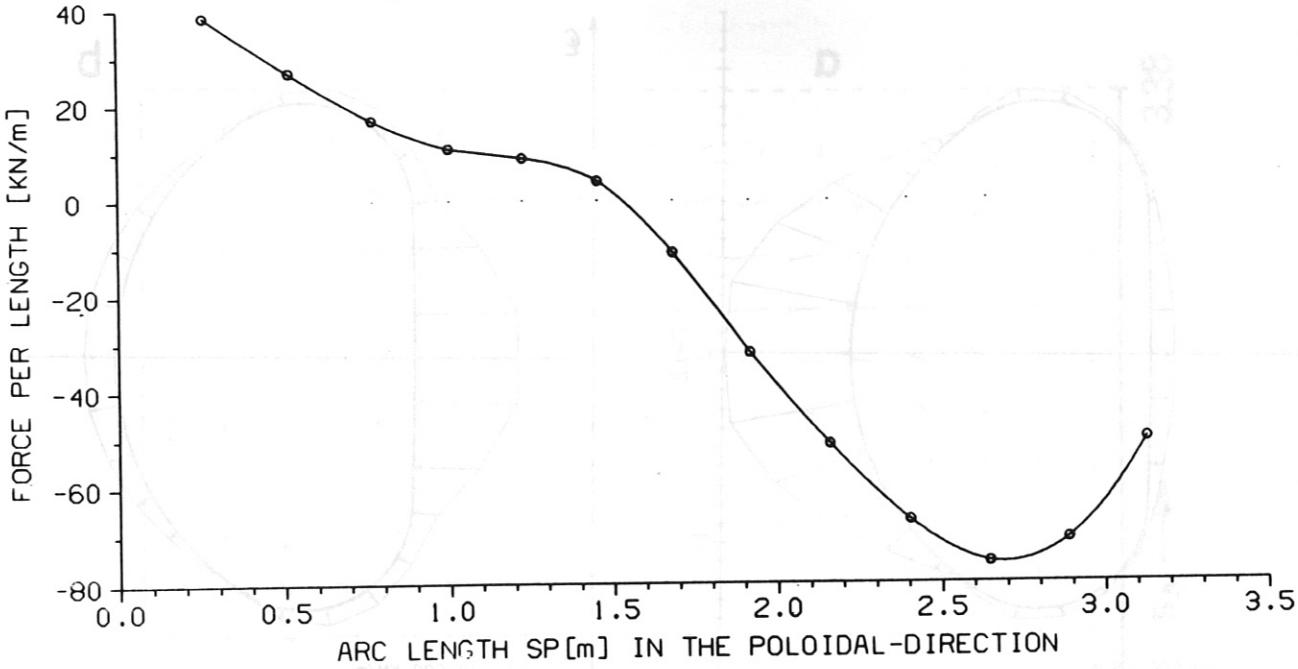

Fig. 12. Distribution of the poloidally directed total force F_ϑ on segment 1 (L configuration).

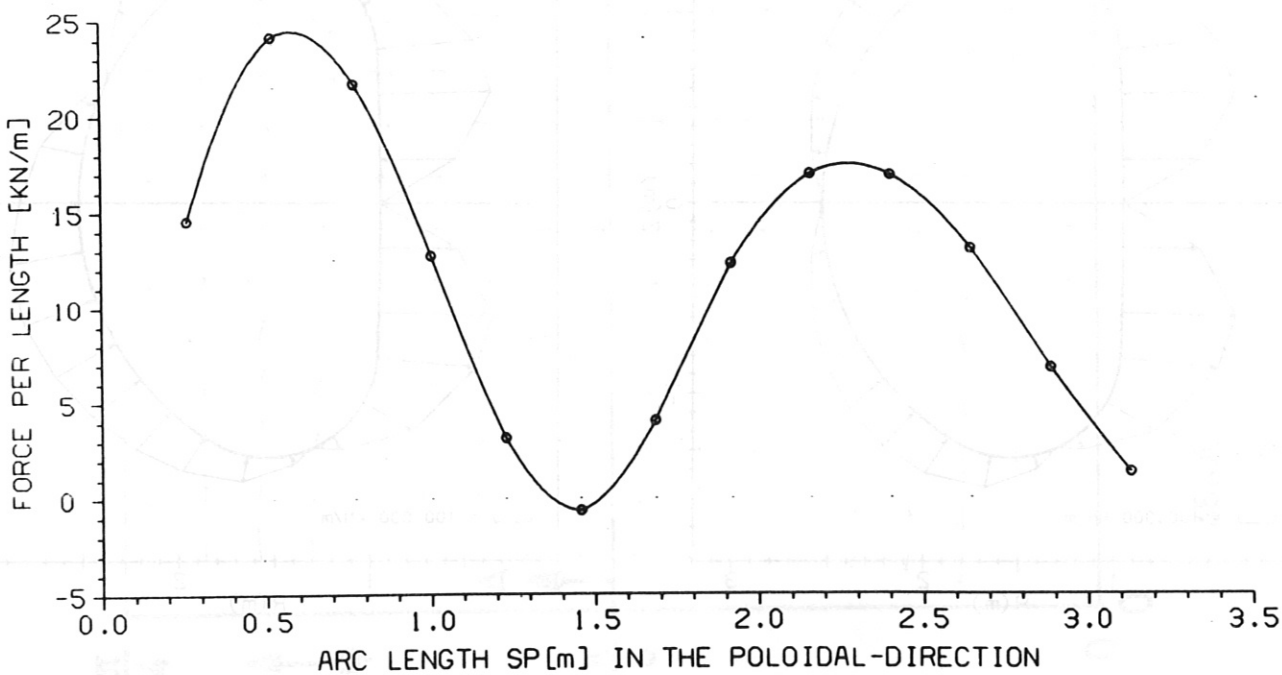

Fig. 13. Distribution of the toroidally directed total force F_φ on segment 1 (L configuration).

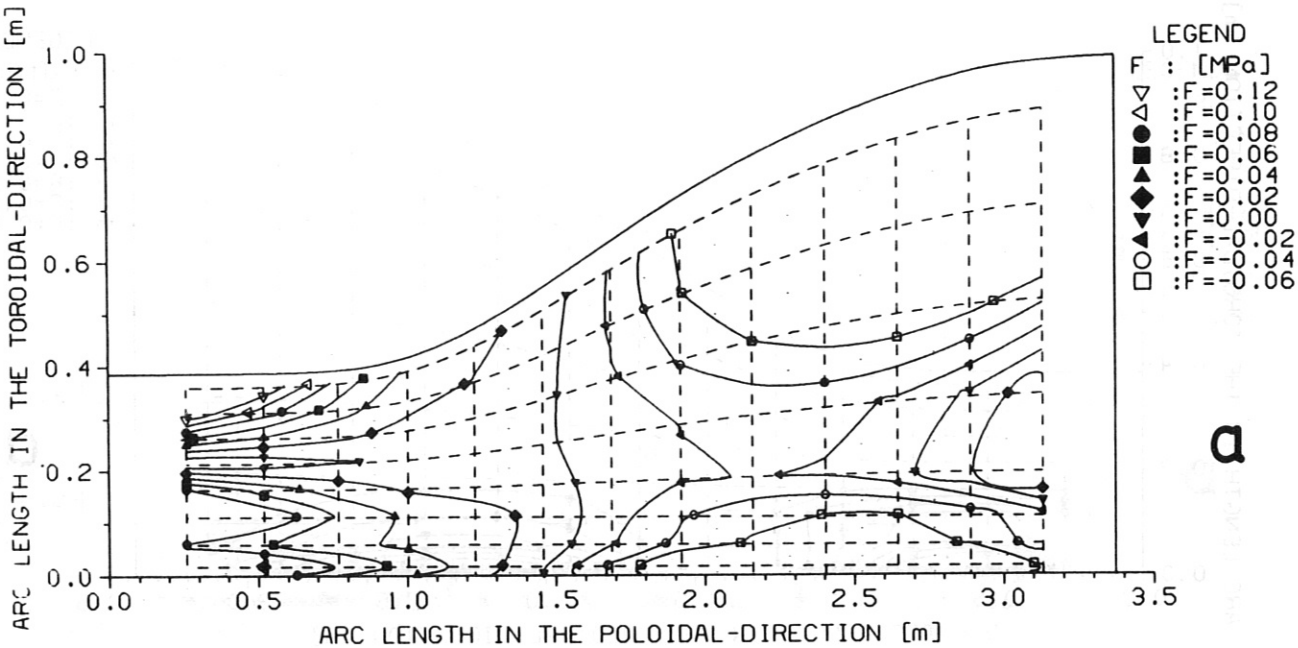

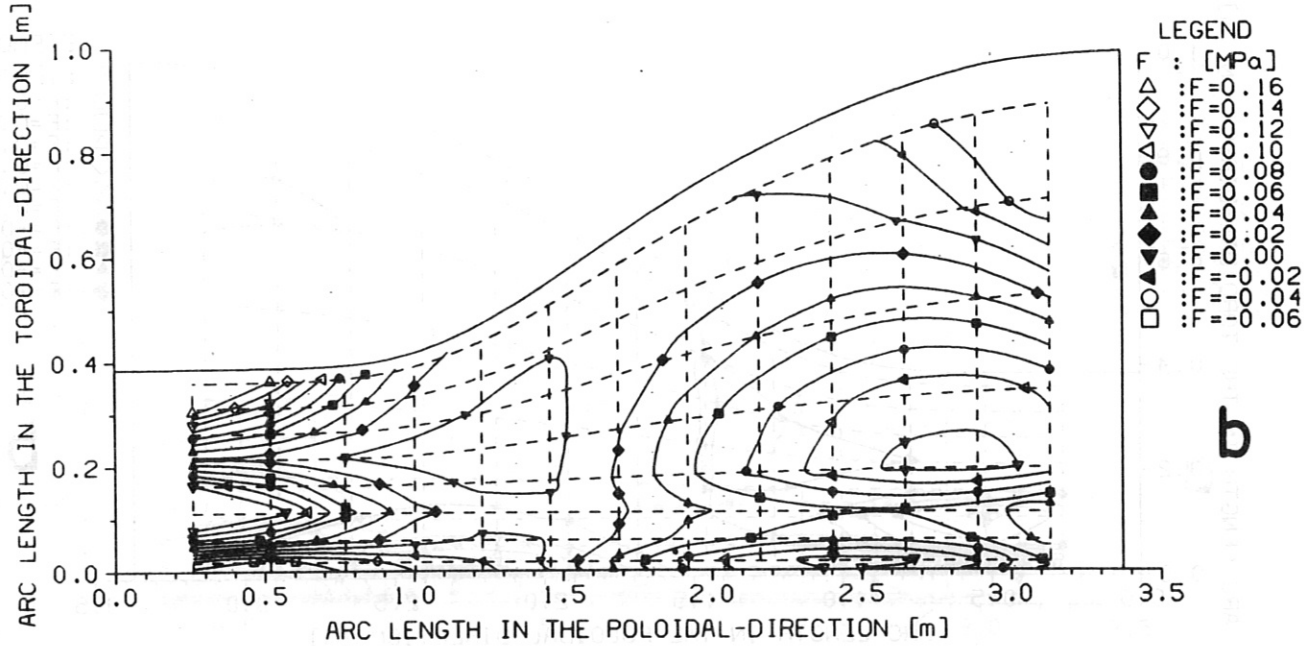

Fig. 14. Contour lines of the total force F_ϑ (L configuration): a on the top half of segment 1, b on the bottom half of segment 1.

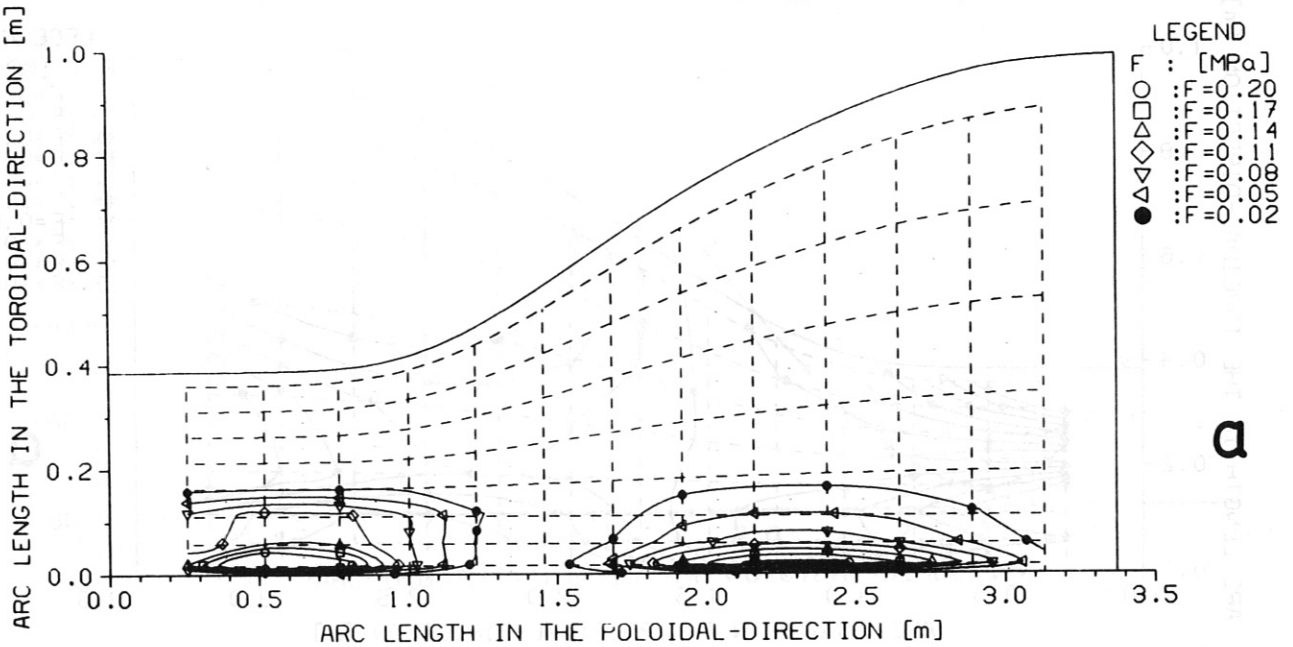

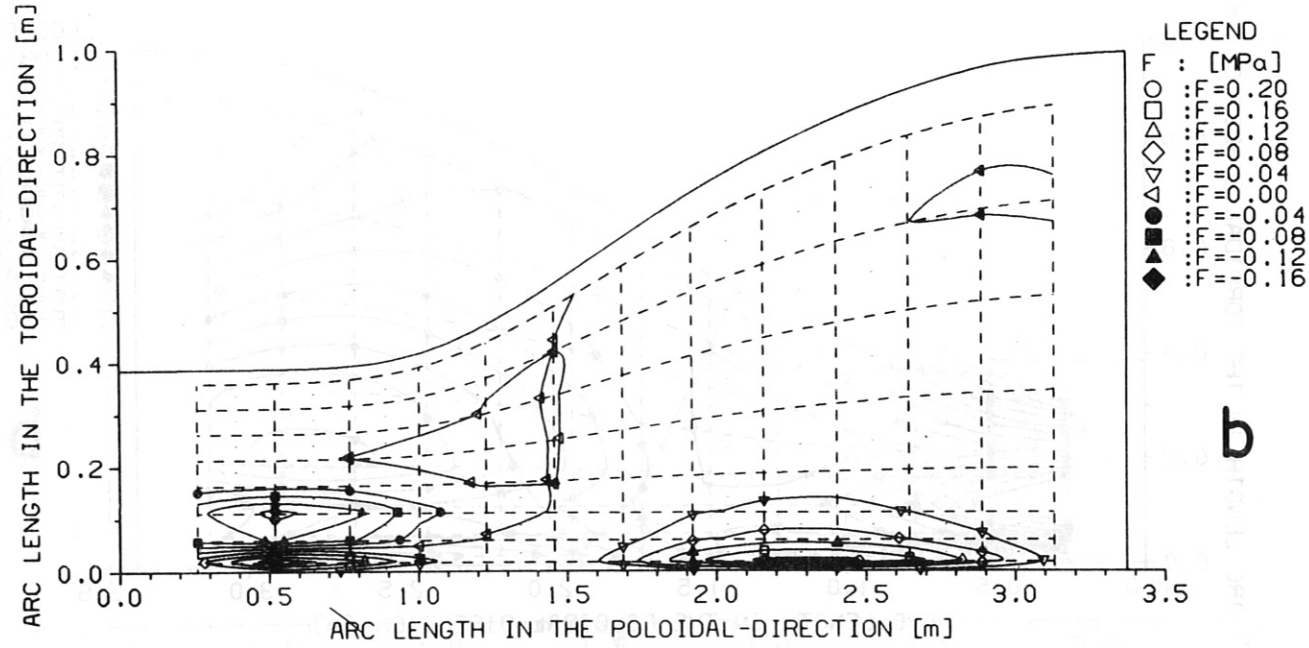

Fig. 15. Contour lines of the total force F_φ (L configuration): a on the top half of segment 1, b on the bottom half of segment 1.

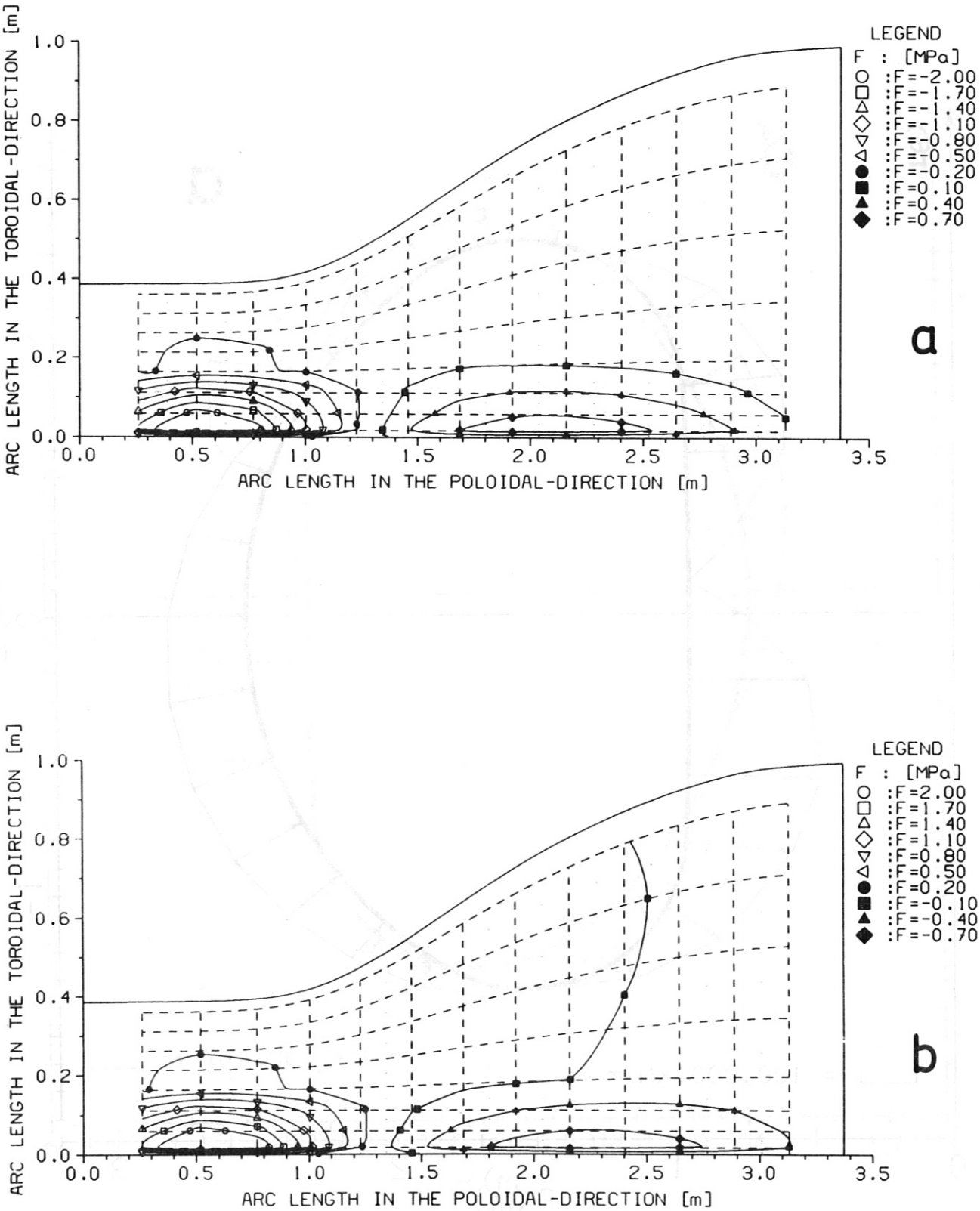

Fig. 16. Contour lines of the total normal force F_n (L configuration): a on the top half of segment 1, b on the bottom half of segment 1.

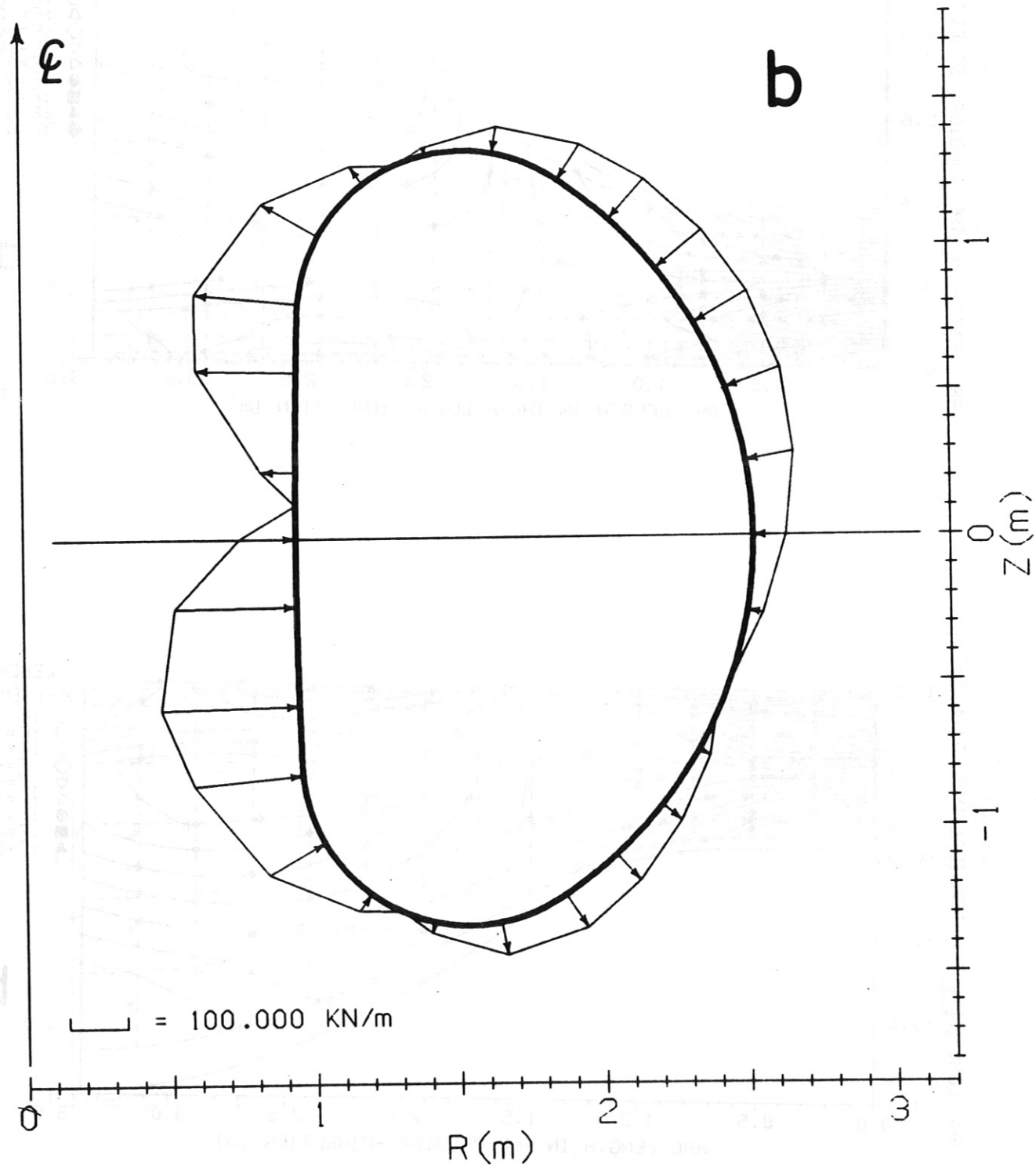

Fig. 17. Distribution of the total normal force F_n (SN configuration): a on segment 1, b on segment 16.

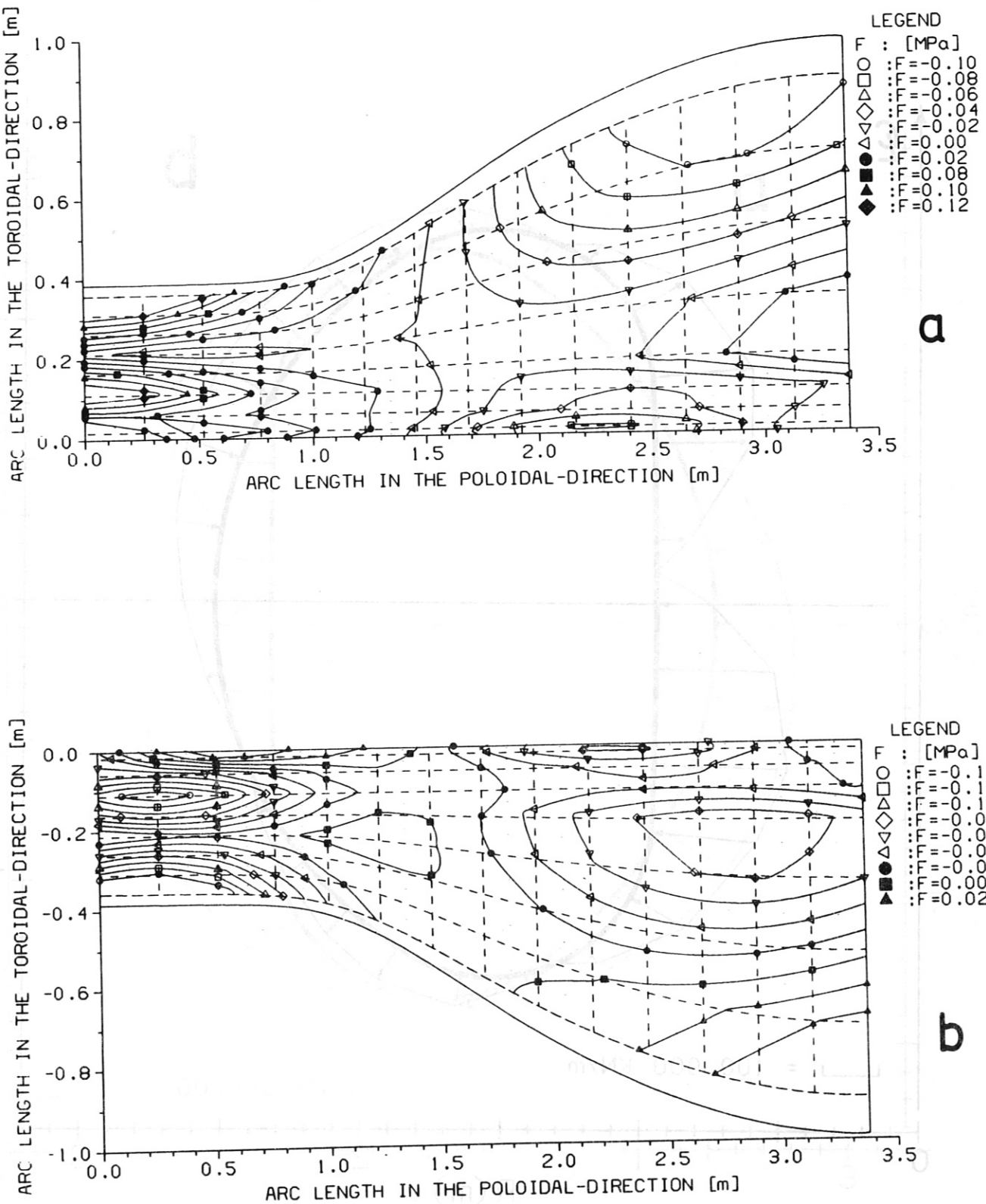

Fig. 18. Contour lines of the total force F_ϑ (SN configuration): a on the top half of segment 1, b on the top half of segment 16.

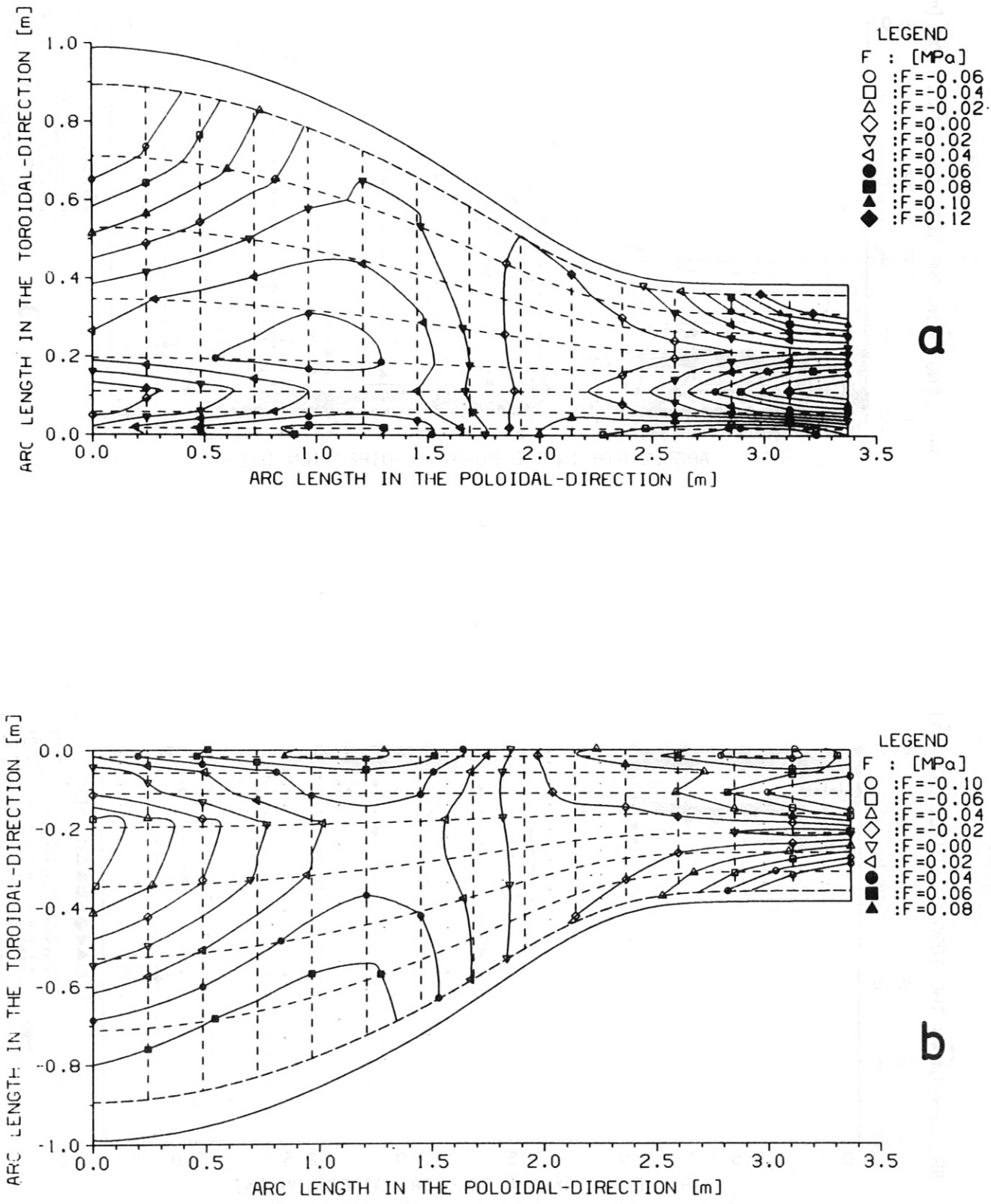

Fig. 19. Contour lines of the total force F_ϑ (SN configuration): a on the bottom half of segment 1, b on the bottom half of segment 16.

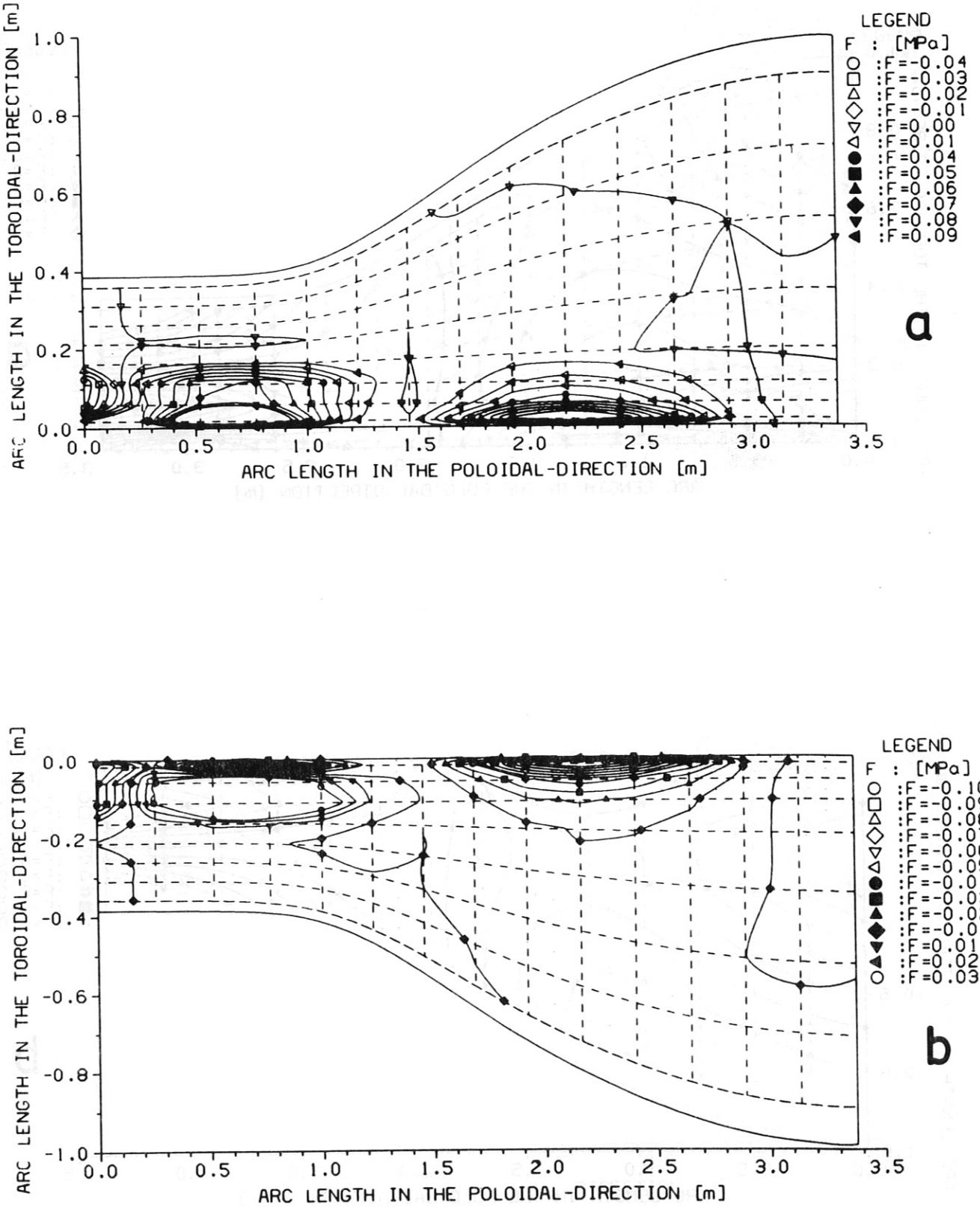

Fig. 20. Contour lines of the total force F_φ (SN configuration): a on the top half of segment 1, b on the top half of segment 16.

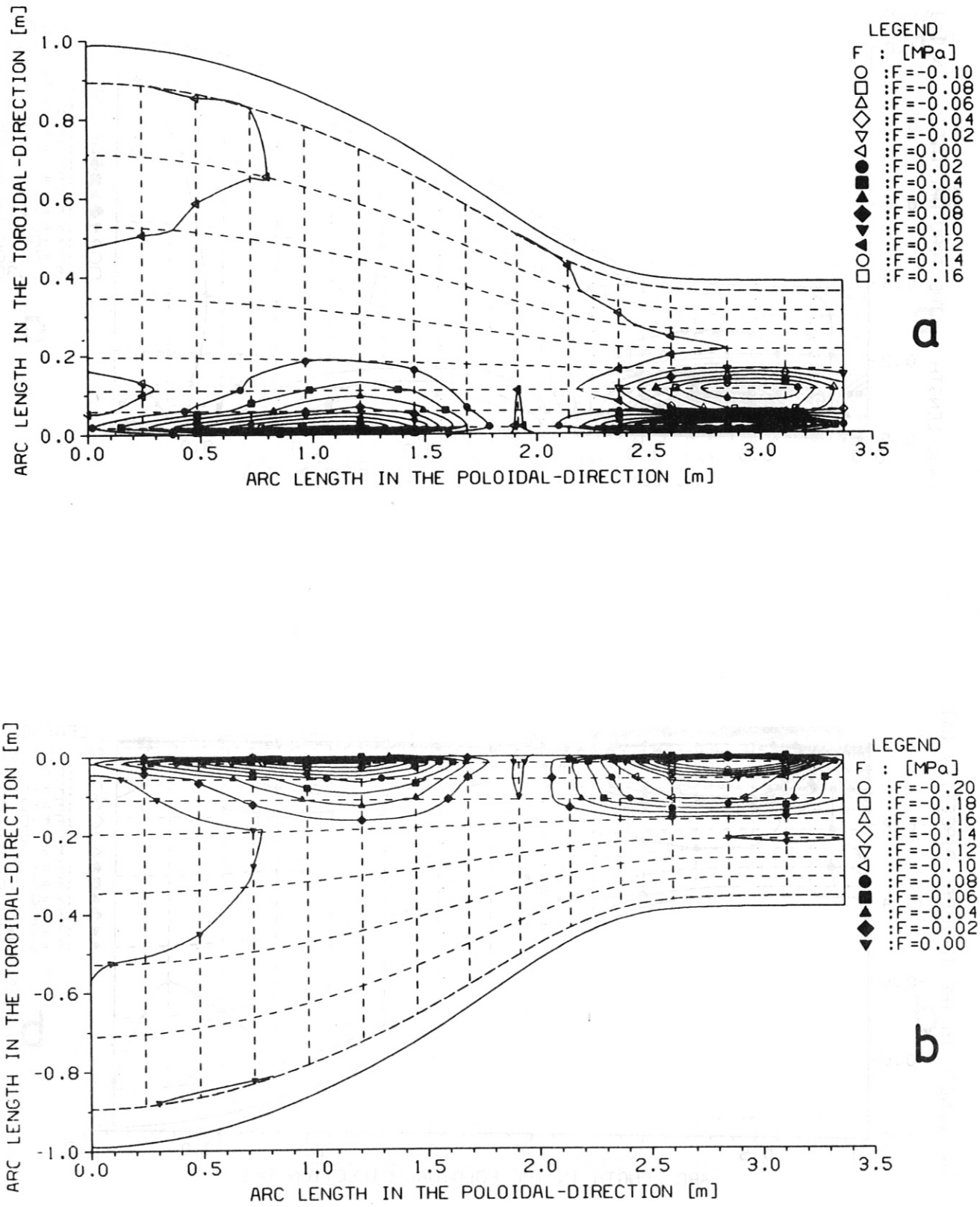

Fig. 21. Contour lines of the total force F_φ (SN configuration): a on the bottom half of segment 1, b on the bottom half of segment 16.

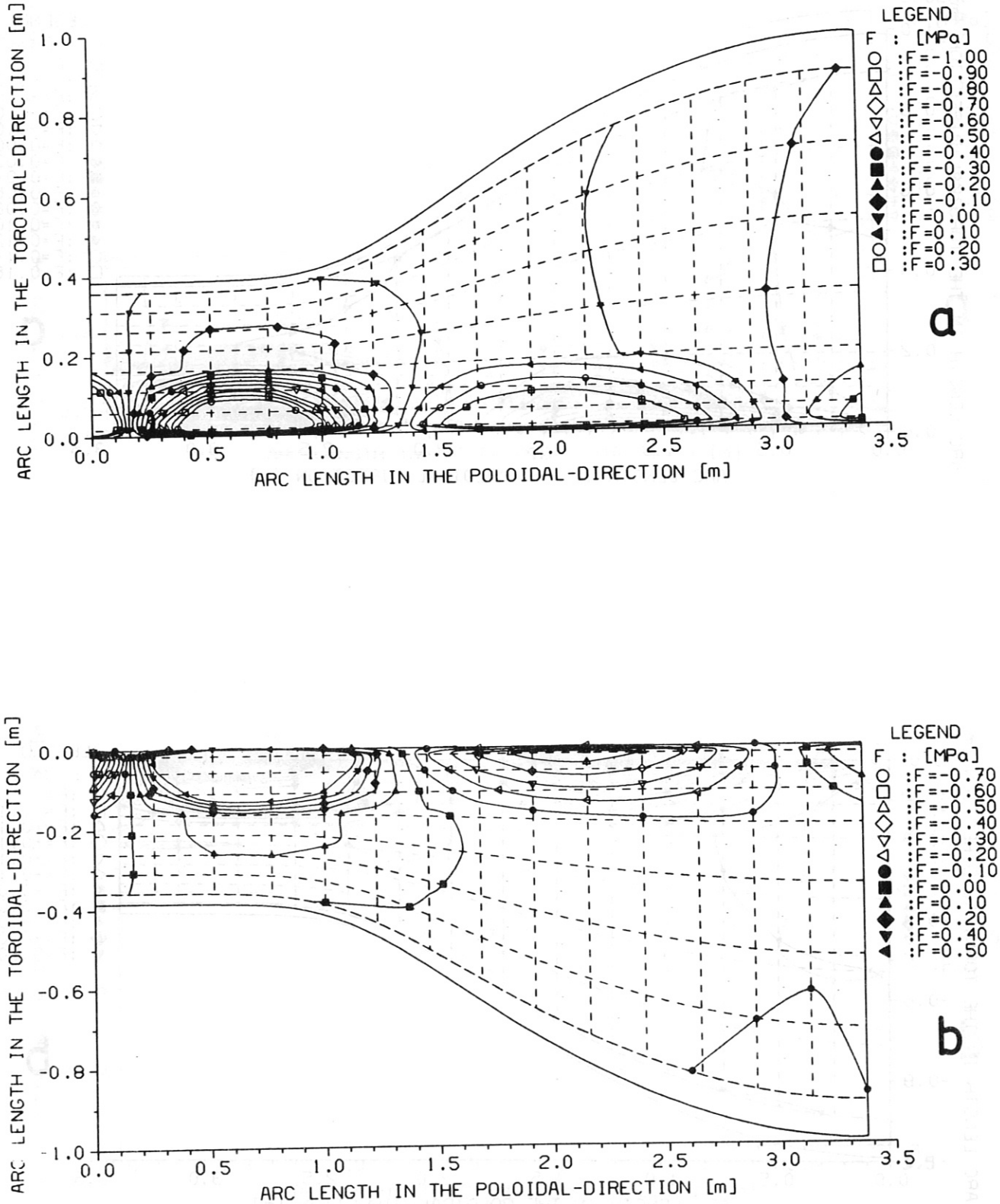

Fig. 22. Contour lines of the total normal force F_n (SN configuration): a on the top half of segment 1, b on the top half of segment 16.

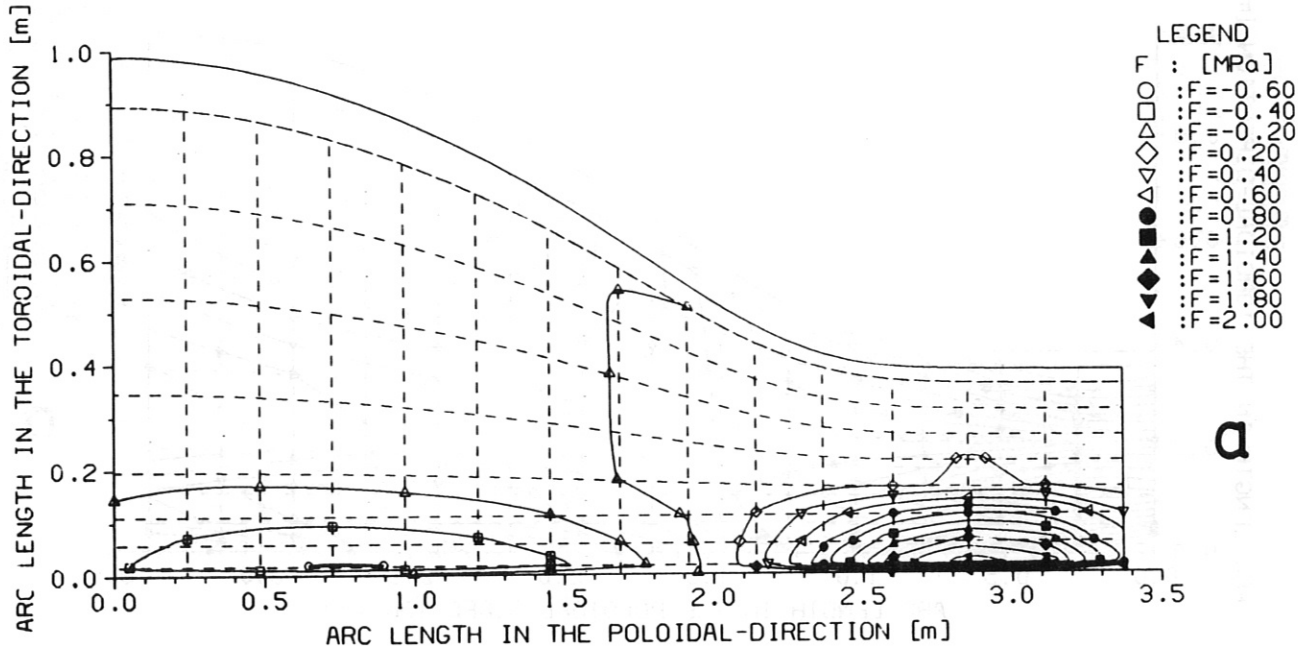

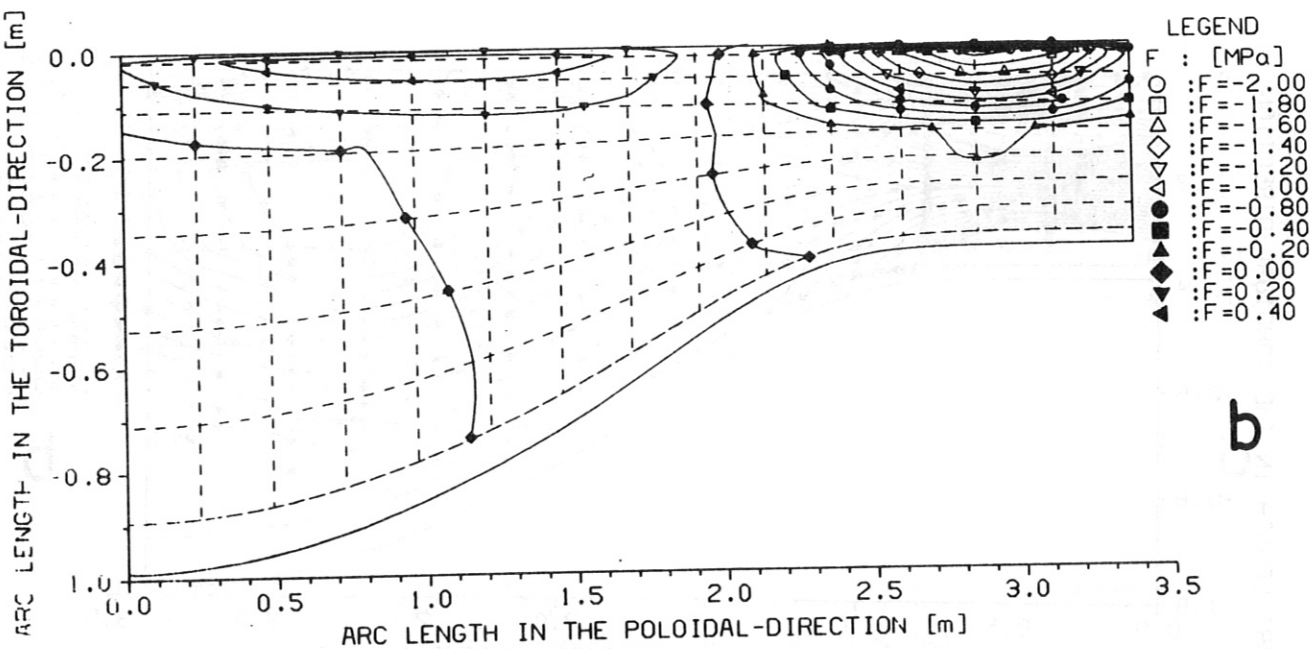

Fig. 23. Contour lines of the total normal force F_n (SN configuration): a on the bottom half of segment 1, b on the bottom half of segment 16.

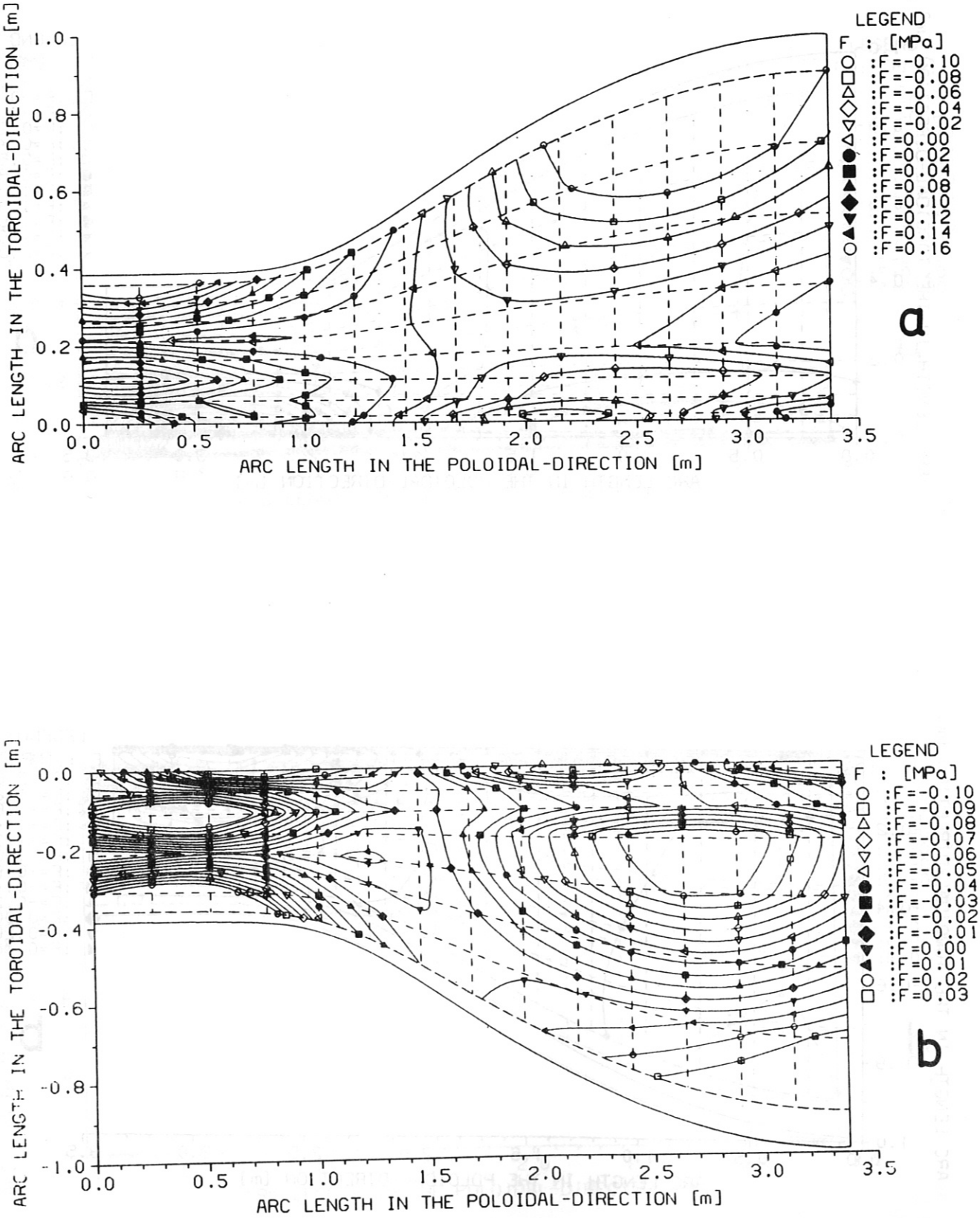

Fig. 24. Contour lines of the total force F_ϑ (displaced SN configuration): a on the top half of segment 1, b on the top half of segment 16.

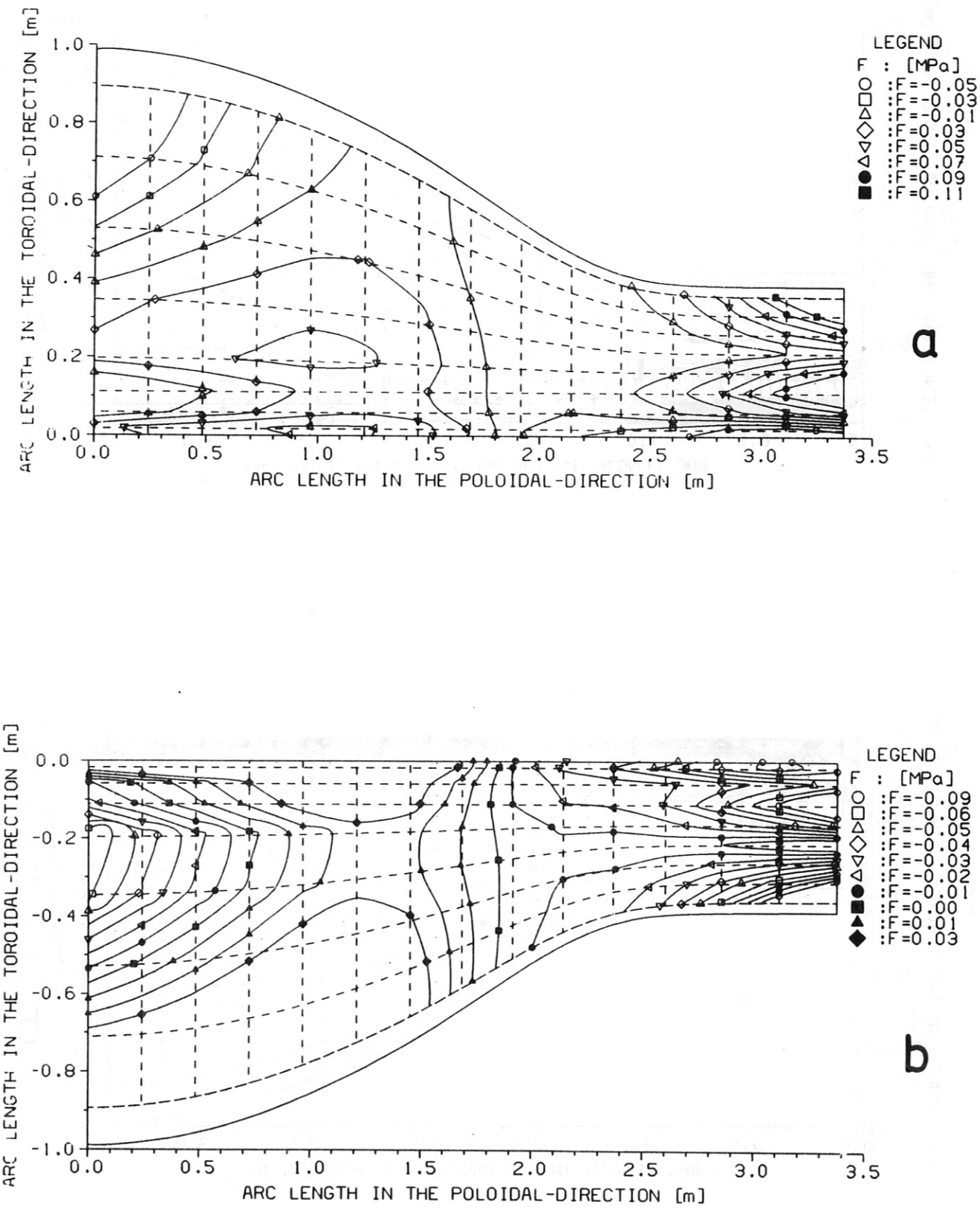

Fig. 25. Contour lines of the total force F_ϑ (displaced SN configuration): a on the bottom half of segment 1, b on the bottom half of segment 16.

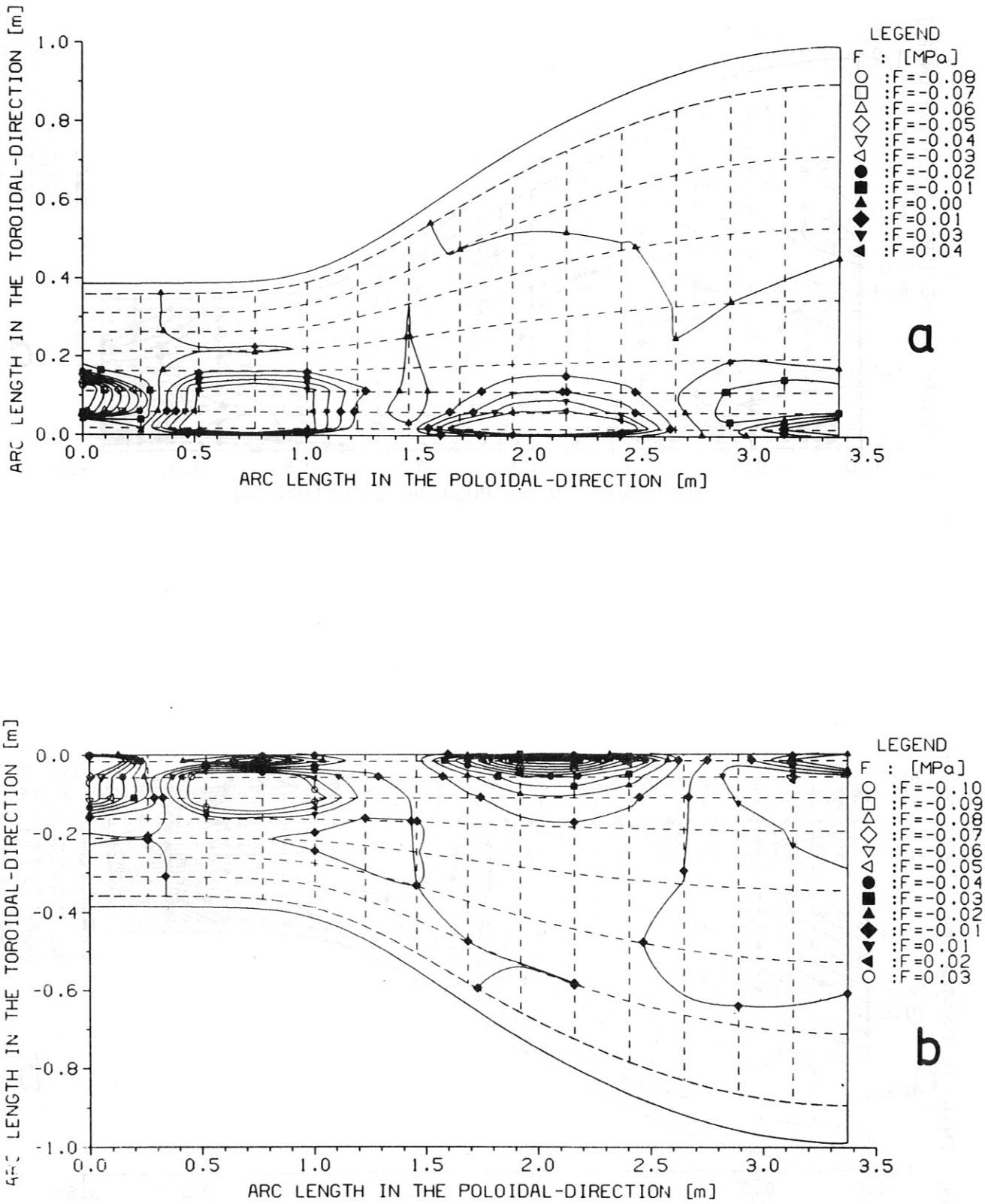

Fig. 26. Contour lines of the total force F_φ (displaced SN configuration): a on the top half of segment 1, b on the top half of segment 16.

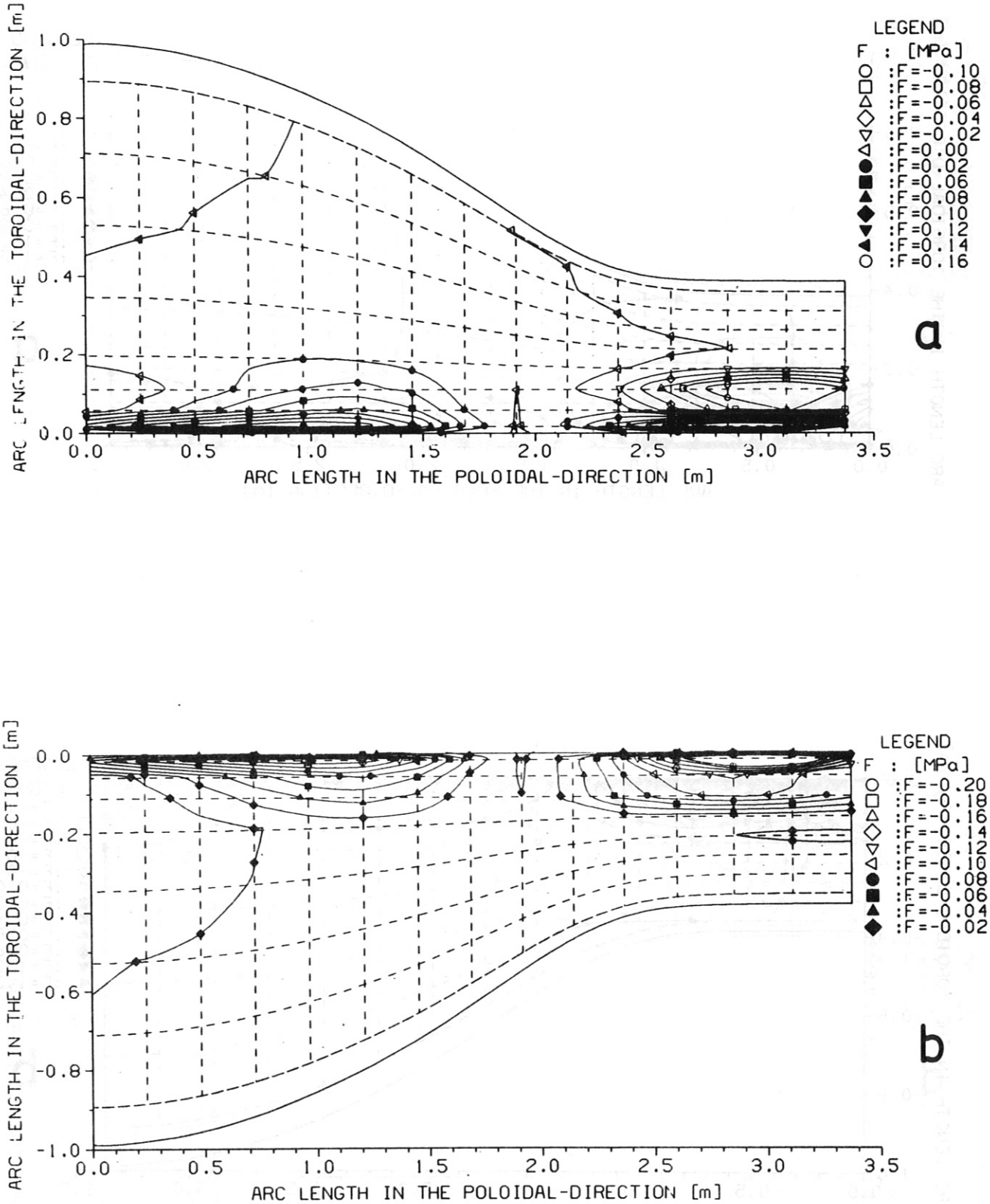

Fig. 27. Contour lines of the total force F_φ (displaced SN configuration): a on the bottom half of segment 1, b on the bottom half of segment 16.

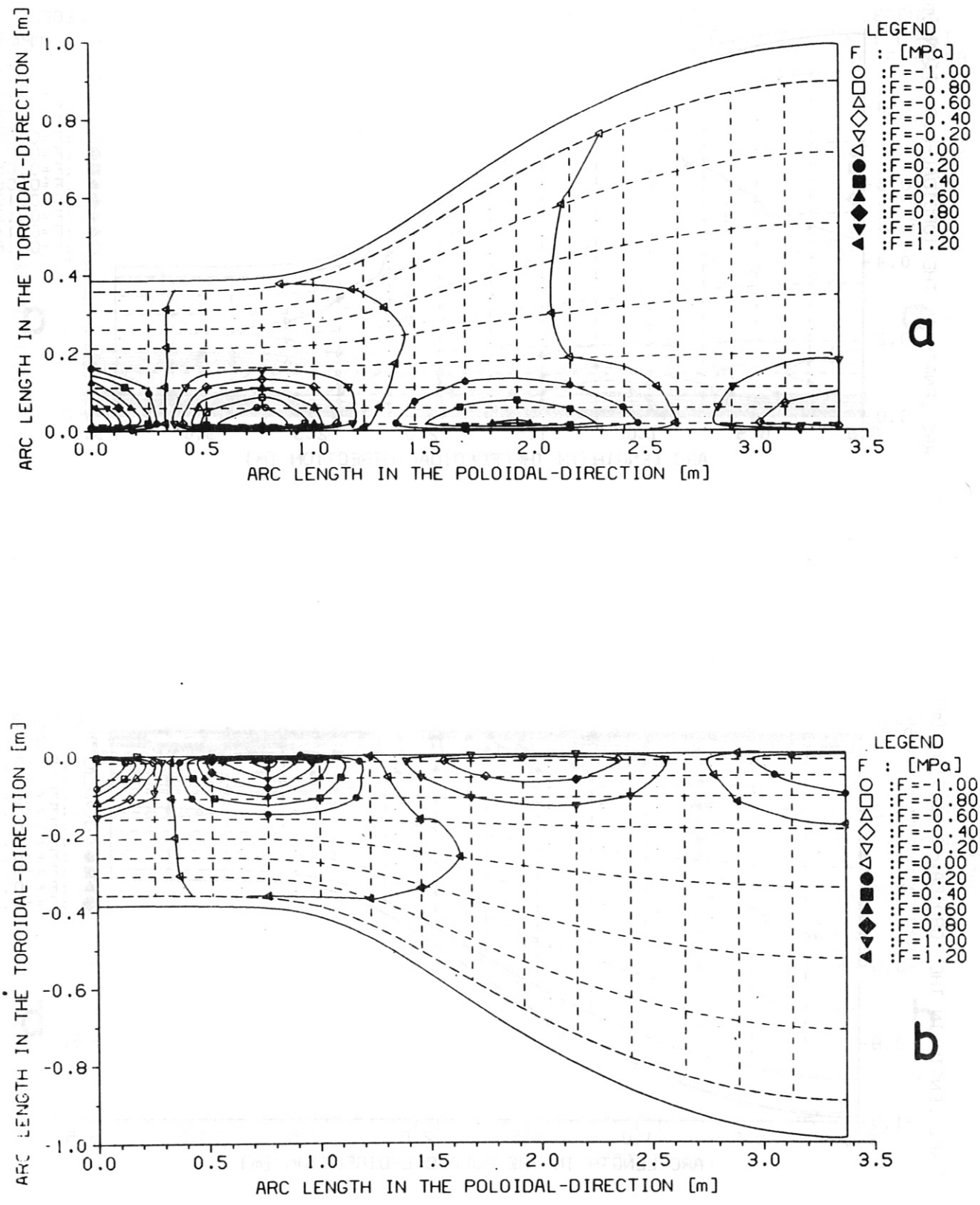

Fig. 28. Contour lines of the total normal force F_n (displaced SN configuration): a on the top half of segment 1, b on the top half of segment 16.

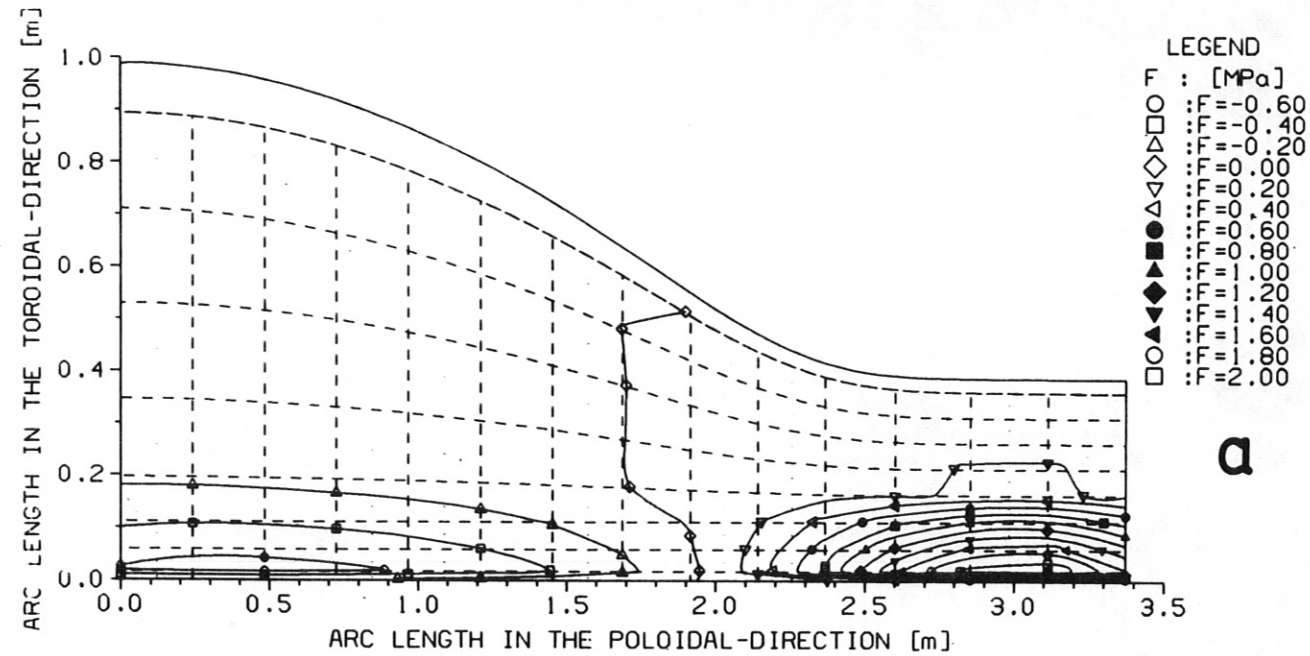

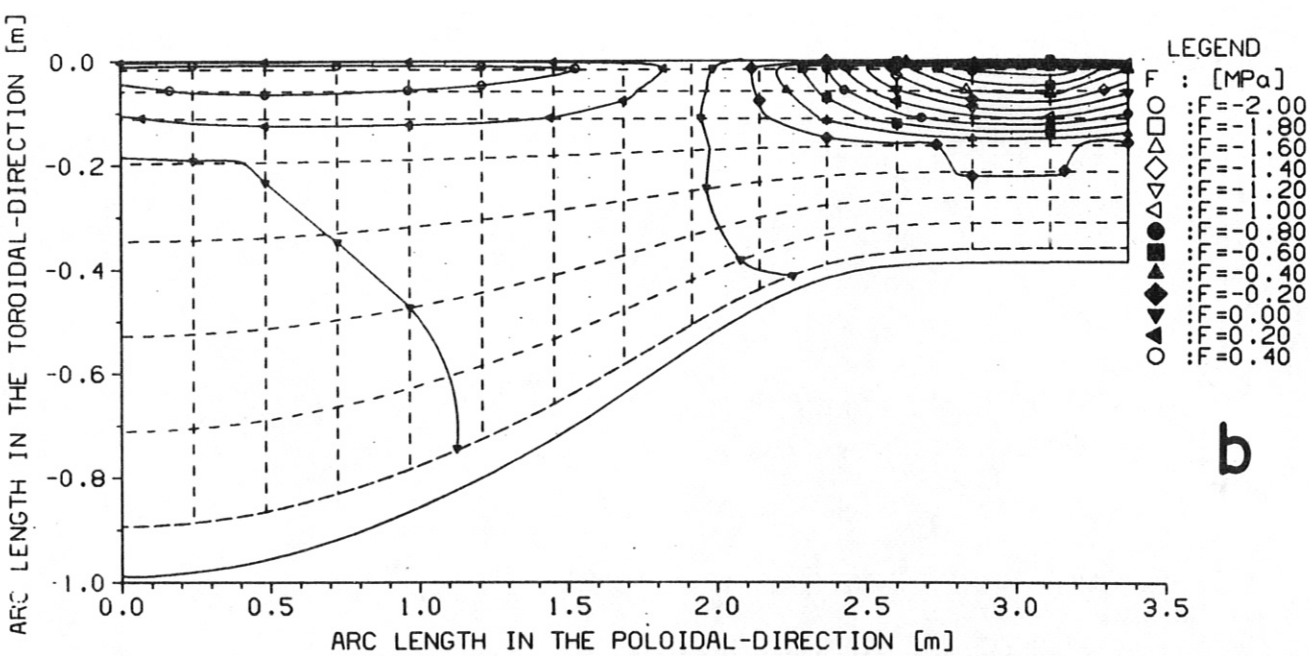

Fig. 29. Contour lines of the total normal force F_n (displaced SN configuration): a on the bottom half of segment 1, b on the bottom half of segment 16.